Earth-Science Reviews 203 (2020) 103143

Contents lists available at ScienceDirect

Earth-Science Reviews

journal homepage: www.elsevier.com/locate/earscirev

A review on freeze-thaw action and weathering of rocks

Maxim Deprez[a,*], Tim De Kock[a,b], Geert De Schutter[c], Veerle Cnudde[a,d]

[a] PProGRess/UGCT, Department of Geology, Ghent University, Krijgslaan 281 (S8), 9000 Gent, Belgium
[b] Antwerp Cultural Heritage Sciences (ARCHES), University of Antwerp, Blindestraat 9, 2000 Antwerp, Belgium
[c] Magnel-Vandepitte Laboratory, Department of Structural Engineering and Building Materials, Ghent University, Technologiepark-Zwijnaarde 60, 9052 Gent, Belgium
[d] Chairholder "Porous media imaging techniques", Department of Earth Sciences, Utrecht University Princetonlaan 8a, 3584 CB Utrecht, the Netherlands

ARTICLE INFO

Keywords:
Frost damage
Ice crystallization
Weathering
Pore scale
Geomaterials

ABSTRACT

Freeze-thaw weathering is an important surface process and the complex underlying processes can be understood as an interplay between rock properties and its dynamic environment. Multiple researchers coming from different scientific disciplines have contributed to the present-day knowledge on the matter and misconceptions still prevail. In a changing climate, the multidisciplinary insights into freeze-thaw action are crucial for a better understanding of rock weathering in natural and anthropogenic environments. In this review, a series of laboratory and in-situ field tests are presented to illustrate the present-day methods to assess freeze-thaw weathering. Over the last century, these methods led to insights and the development of theories on damage mechanisms. Presently, it is accepted that crystallization pressure is responsible for the majority of stresses in the material's pores. Damage is induced when these stresses overcome the local tensile strength. Since most of the methods used to derive and validate stress build-up theories are indirect observations of parameters related to the phase transition, it is hard to reach a consensus on the exact explanation for stress development. Direct observations, which require actual real-time observation of the pore space during a freeze-thaw cycle, are therefore favoured to reach agreement. Eventually, the goal is to achieve a better insight on which processes potentially occur, how these vary with different environmental, temporal and spatial conditions and under which circumstances damage is inflicted.

1. Introduction

Freeze-thaw (FT) weathering is one of the most important factors in deterioration of rocks and other porous geomaterials in areas where the temperature periodically fluctuates around the freezing point (e.g. Matsuoka and Murton, 2008). When the temperature drops below the freezing point, moisture bearing materials will be subjected to internal stresses caused by the phase transition from water to ice (Winkler, 1968). These stresses are consequently released during thawing. In natural circumstances, most materials will not disintegrate due to one FT cycle, but sequential FT loading will cause deterioration of the porous subjects. Generally, by subsequent freezing and thawing, the materials gain in porosity through the introduction of micro-cracks (Martinez-Martinez et al., 2013). This is expressed in overall weakening of material. At the same time, aesthetic problems arise when for example building stones lose grains, flakes or crumbles from the outer surface as a consequence.

Because of the wide importance of FT weathering, this phenomenon has been extensively studied in different fields of research, such as geology, soil science, physics, geomorphology, geo- and civil engineering. Mostly studied materials include natural building stones, soils and bedrock, but also extensive research has been performed on engineered cementitious materials, such as concrete and mortars, and ceramics. In the case of soils, the aggregates of which they consist are broken up by ice formation (Oztas and Fayetorbay, 2003), causing changes in the chemical (Koponen and Martikainen, 2004), physical (Dagesse, 2013) and biological (Feng et al., 2007) properties of the soil. In periglacial environments, frost heave of soil due to the development of ice lenses (Peppin and Style, 2013; Taber, 1930, 1929) results in the breakdown of structures, such as roads, railways, pipes, pavements and buildings. Moreover, frost action can be considered one of the major agents to disintegrate solid bedrock into transportable sediments (Anderson, 1998; Matsuoka and Murton, 2008). Through the production of a loose top layer of rock fragments, FT weathering indirectly contributes to hazards, such as rock falls, rock slides and debris flows (Matsuoka and Sakai, 1999). These hazards are able to damage infrastructure, block rivers and roads, and are an immediate danger to human lives.

* Corresponding author.
E-mail address: maxim.deprez@ugent.be (M. Deprez).

https://doi.org/10.1016/j.earscirev.2020.103143
Received 18 February 2019; Received in revised form 14 February 2020; Accepted 21 February 2020
Available online 22 February 2020
0012-8252/

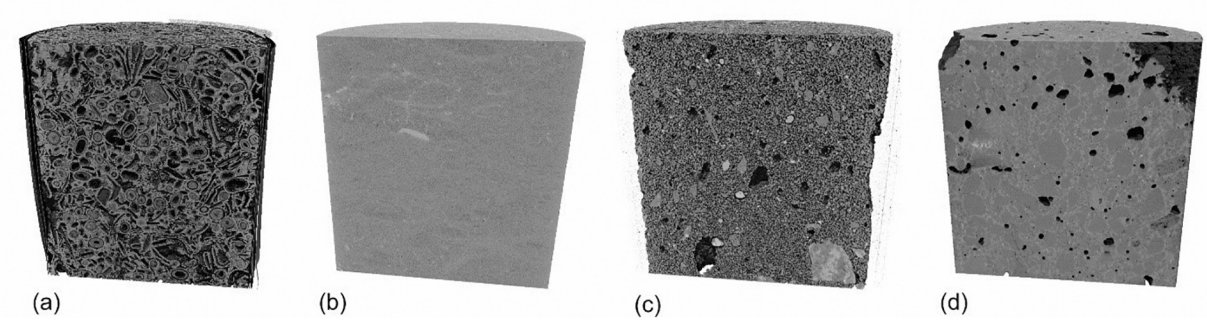

Fig. 1. 3D renderings of X-ray micro computed tomography (μCT) data from four different porous materials, explanatory for the different pore sizes and structures materials can have. (a) a porous (30%) limestone, (b) a low porous (2%) limestone with no visible pores, (c) a brick (32% porous) with a variety of visible pore sizes and (d) mortar (18% porous) with visible air voids and invisible capillary pores. (a), (c) and (d) have sample diameters of 1 cm and were imaged with a resolution of 7 μm. The limestone in (b) was 2 cm in diameter and imaged with a spatial resolution of 15 μm. The spatial resolution restricts visualization and quantification of smaller pores.

Regions prone to FT weathering are closely related to the global climate. As the latter is changing, regions affected by this weathering phenomenon will change accordingly. For a certain area, these changes comprise differences in temperature range, duration and frequency of FT events. Soil, for example, can lose some of its insulation due to a decreasing thickness of the overlying snowpack, causing an increased sensitivity to FT events (Henry, 2007). Also in mountainous areas, the change in FT activity has an impact on the sediment delivery downslope (e.g. Anderson et al., 2013; Sass and Oberlechner, 2012). Through global warming, buildings and archaeological remains in Western Europe are expected to be less affected by FT events in the future while the occurrence of these events will increase in areas of high altitude and/or latitude (Grossi et al., 2007). Differences in FT risk can also be found on a regional scale (Lisø et al., 2007) and more local scale, influenced by e.g. the urban heat island or the location within a building (Guilbert et al., 2019; McAllister et al., 2013; Vandemeulebroucke et al., 2019).

In the presently changing climate, it is expected that the employed materials are more durable, which implies they need to have a prolonged service life. Therefore, degradation due to FT episodes is highly undesirable. Moreover, buildings have to be energy-efficient and, for this reason, insulation is most often placed either inside or outside the outer bearing walls. Interior insulation, however, leads to an inefficient drying of the outer walls, which might accelerate the FT weathering of the wall (Künzel, 1998; Vandemeulebroucke et al., 2019; Vereecken et al., 2015). Consequently, construction materials are necessarily highly FT resistant in sensitive areas, and, moreover, they need to endure future environmental changes, such as change in atmospheric humidity and temperature.

Damage by FT action is presently mainly attributed to crystallization pressure (Everett, 1961; Scherer, 1999; Steiger, 2005a, 2005b; Steiger et al., 2014; Walder and Hallet, 1985). Also volumetric expansion (Hirschwald, 1908) and hydraulic pressure theory (Powers, 1945) have been used as mechanisms for stress generation. Most poromechanical models actually attribute the largest part of the stress to hydraulics (Coussy and Monteiro, 2007; Eriksson et al., 2018; Koniorczyk et al., 2015) and it is also proposed that the freezing of isolated pockets of water could inflict a considerable amount of pressure (Chatterji, 1999). All theories are based on thermodynamic and/or poromechanical models and are validated by indirect methods, such as the measurement of length changes. Most recent experiments interpret the crystallization pressure as main mechanism from the observations (De Kock et al., 2015; Ruedrich and Siegesmund, 2007).

Extensive research has been performed on FT weathering in multiple scientific disciplines and each discipline has its own scale on which FT processes are acting and consequently also its own methods to tackle FT related phenomena. Therefore, a multidisciplinary framework that enables scientists to continue fundamental research on the acting damage mechanisms is built in this review. Frost susceptibility is related to different material properties, and therefore, this review begins with a description of those properties of three heavily studied main classes of porous solids, which are natural stones, cementitious materials and ceramics. Despite the focus of this review lies on these rigid materials, the processes occurring during ice crystallization are equally valid for less rigid materials, such as soils. An overview on the different damaging mechanisms proposed throughout the last century is given before proceeding to a theoretical background on thermodynamics during growth of ice in pores and the resulting pressures. Next it is discussed how these pressures can lead to FT damage patterns. Subsequently, different methods to investigate FT processes are elucidated. Since a number of environmental and material parameters can vary both in the lab and on the field, a closer look is taken at the influence of these parameters on the behaviour towards FT weathering. Finally, special attention is given to the potential and recent developments of pore-scale imaging (e.g. De Kock et al., 2015) as well as the future possibilities of these techniques in resolving remaining issues in FT research.

2. Structure of porous mineral materials

Weathering studies essentially have three main attributes: material properties, moisture conditions and thermal conditions (Hall, 1999). Whereas the latter two factors are highly variable and environmentally related, the material properties can be defined quite accurately. These properties, such as pore-size distribution, strength and elastic moduli all link back to the structure of the material, which consists of two main parts: the solid phase and the pores. The solid phase is mostly responsible for the mechanical strength of a building material, which is assumed to be governed by strength of the mineral phases present and extent of bonding or cementation (Merriam et al., 1970). The characteristics of the pores, such as the total pore volume, size, shape and connectivity, will determine the conditions for fluid transport within the subject (Hall and Hoff, 2002). The magnitude and the location of internal stresses, caused by ice crystallization, then again depend on the pore characteristics. Hence, the combination of both solid phase and pores, as present in the structure, will determine the weathering behaviour (Benavente et al., 2004; Maage, 1984). As the origin of porous mineral materials is very diverse, the internal structure varies widely (Figs. 1 and 2), as does frost susceptibility. It is necessary to give an overview of the different kinds of materials and their structure to understand their mechanical properties and, consequently, their weathering behaviour.

Rocks can be of sedimentary, magmatic or metamorphic origin, with their structure or fabric defined by the geological formation process. Magmatic rocks are composed of angular mineral grains which have interlocked during crystal growth from a melt. Their mechanical

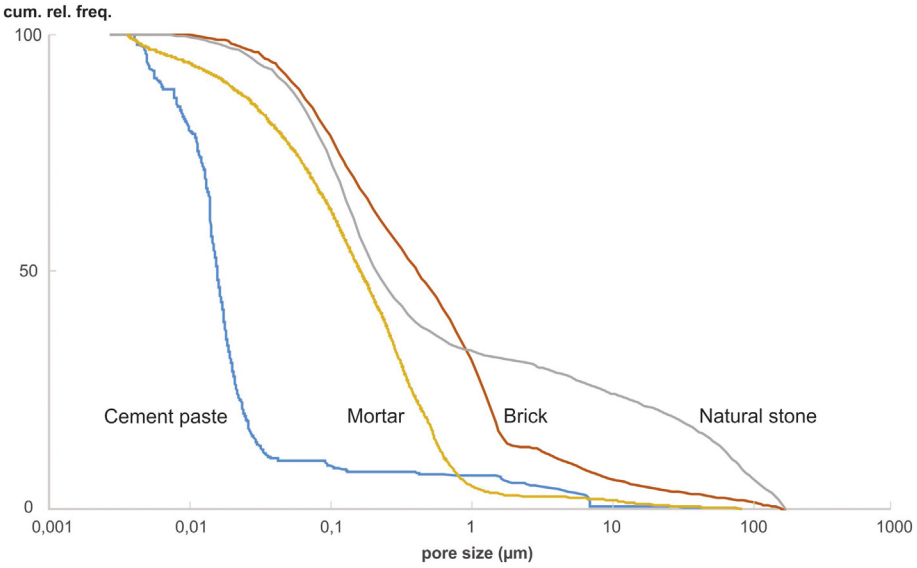

Fig. 2. Examples of pore-size distributions of four different building materials determined by mercury intrusion porosimetry (MIP) displayed as cumulative relative frequencies (cum. rel. freq.) of pore sizes between 1 nm and 100 µm. Due to this limit in detection of the MIP technique, air voids in cement paste and mortars and other large pores in bricks and natural stones (Fig. 1) are not incorporated. The natural stone (sandy limestone, data from De Kock et al. (2017)) clearly shows a larger fraction of relatively large pores, while the pores in cement paste are clearly in the nanometre range (data from Snoeck (2016)). Natural stone, brick and mortars all show a large fraction of pores between 1 and 0.1 µm.

strength is determined by the degree of interlocking of the grains, which relies on their size and shape and the overall mineralogy (Merriam et al., 1970). Here, pores are most commonly inter-granular and intra-granular fissures, nanometric to micrometric in size (Mosquera et al., 2000). The combination of strong crystal interlocking and relatively low porosity (< 5% (Vosteen and Schellschmidt, 2003)) causes relative large mechanical strength. Metamorphic rocks are somewhat similar to magmatic rocks, with a strong mineral interlocking and a low porosity. However, some minerals, such as micas, are frequently aligned in the direction perpendicular to the largest pressure component during their formation. This oriented fabric often serves as preferential weakness planes, which needs to be considered when metamorphic rocks are used as building stones (Shea and Kronenberg, 1993). Of all rock types, sedimentary rocks are the most variable in structure. In general, sandstones and limestones are often used for building purposes due to their workability and availability and these are therefore dominant in FT studies on building stones. These rocks can consist of mineral grains, fossils and lithic fragments, which are bonded either by their original sedimentary matrix, by precipitation of a natural cement, by pressure-induced interconnection between different components or by a combination. The natural cement consists mostly of calcite and quartz and the cement structure depends on the ion-rich solution and diagenetic conditions during precipitation. The porosity of sedimentary rocks ranges from almost zero to over 50%. Since calcite components are prone to dissolution, relative large holes caused by this process (secondary porosity) are not rare in calcareous rocks. Also partial cementation causes the occurrence of large pores within the uncemented rock parts. Mineral grains and the natural cement can have pores in the nanometre scale, while the pore size within fossils can vary from the nanometre to the centimetre scale. Hence, even within one rock, the porosity can vary largely, and the pore-size can range from nanometre to centimetre scale with unimodal to multimodal distributions (Figs. 1 and 2). Characterising the structure of a these rocks therefore often needs to be performed from nano- to macroscale (De Boever et al., 2015).

Concrete and mortar are composed of mineral grains, or aggregates, with a certain specified grain-size distribution, so that the cavities between coarser grains are filled by finer grains. The remaining space is then filled with cement paste, a mixture of reactive cement powder and water, which interlocks the aggregates during hardening. This structure causes mortar and concrete compositions to have a high compressive strength. The pore system is determined by the reaction between the cement minerals and water, which forms calcium silicate hydrates (C-S-H). The porosity of fully hydrated cement paste is 28% (Hall and Hoff, 2002; Powers and Brownyard, 1946), however, not all cement is able to react with the water and a part of the liquid will therefore stay in the volume as the cement hardens. Through this process, capillary pores (10 µm – 10 nm) are created in the structure. Gel pores are even smaller (10–0.5 nm) and form the space between C-S-H bindings (Fig. 1). Also trapped air will be present in the total volume and will be present as relatively large air voids (10 µm – 1 cm). As a result, the pore-size distribution of concrete and mortar is mostly bimodal (Du and Folliard, 2005). The total porosity depends on the amount of water that was used in the total mix. The larger this amount, the more water will be left unreacted causing more capillary pores. In general, the porosities of aggregates are almost negligible compared to that of cement paste. Therefore, the total porosity within concrete or mortar is a trade-off between the volume of cement, water and aggregates. It has been established that an increase in large air void pores can be beneficial when it comes to the FT resistivity (Powers, 1949). However, this increase is disadvantageous for the strength of the material. Therefore, developing a mixture is often a compromise between the strength and the durability requirements.

Ceramics, such as bricks and tiles, are made by heating a clay-based mineral mixture. During heating, interstitial water will evaporate, different mineral phases will partially melt and others will transform into more stable phases for a certain heating temperature. The strength of ceramics is accomplished by a binding material that intertwines the mineral components. This intertwining occurs by the growth of elongated aluminium-silicate clay-derivates, such as mullite, during heating to 1100 °C. The mineral composition of the clay and the firing temperature are important for the internal structure of bricks (Cultrone et al., 2004). In general, bricks produced at a relatively low temperature (i.e. 700 °C) will have a higher porosity, a higher volume of relatively small pores and a lower tensile strength (Maage, 1984). Carbonate-rich clays will cause the largest volume of open pores due to the thermal degradation of calcite. For bricks, a high firing temperature (i.e. 1000 °C) also causes larger rounded pores. In general, the porosity of bricks ranges between 10 and 50% (Hall and Hoff, 2002) with pore sizes varying from the nanometre to the millimetre scale (Figs. 1 and 2) (Coletti et al., 2016).

3. FT damage mechanism theory

3.1. History of FT damage mechanisms

Over the past century, many researchers attempted to explain how exactly this phase transition creates freezing-related stress in the pore

space. Hirschwald (1908) stated that the 9% **volume increase** during the solidification of water was the main cause of frost damage in natural building stones. This implies that when a material is 91% water saturated, the volume increase can no longer be accommodated and the material is supposed to suffer frost damage.

Since frost-induced damage already occurs in porous media with saturation degrees below 91% (e.g. (Fagerlund, 2004; Martinez-Martinez et al., 2013; Prick, 1997; Ruedrich and Siegesmund, 2007), other mechanisms were considered eventually. Powers (1945) argued that volumetric expansion causes unfrozen water to be pushed into the smaller capillary pores. This flux could generate a **hydraulic pressure** that was assumed to exceed the tensile strength of the concrete. This theory enabled Powers (1945) also to explain the higher frost resistance of air-entrained concrete, assuming that the higher concentration of air voids in the air-entrained concrete was able to relief the hydraulic pressure more efficiently. If less air voids are present in the matrix, the risk for higher pressures in the smaller capillaries should increase.

However, contradictory observations caused Powers to review his theory. Powers and Helmuth (1953) reduced the air void spacing to enable an enhanced flux of pore water into the voids. Simultaneous length change measurements revealed a contraction larger than the thermal contraction, while a reduction in expansion by the hydraulic pressure was expected. Moreover, as the cooling was stopped, no relaxation was observed in the concrete with air voids (Fig. 3). According to the hydraulic pressure theory, a stress relaxation should occur as the water makes its way to the large air voids. This led Powers (1975) to withdraw his own theory, although several researchers believe that the hydraulic pressures contribute to the internal stress in several specific cases. Whenever a highly saturated material is sealed off with ice from the outer atmosphere, the water trapped inside could still generate sufficiently high hydraulic pressures to introduce damage (Chatterji and Christensen, 1979). Also, when water-filled pores are surrounded by growing ice crystals, hydraulic pressures can contribute to the internal stresses (Chatterji, 2003). The extent of this hydraulic pressure then relies on the cooling rate, the amount of supercooling prior to nucleation (Sun and Scherer, 2010a) and the pore structure of the cement matrix (De Schutter, 2012).

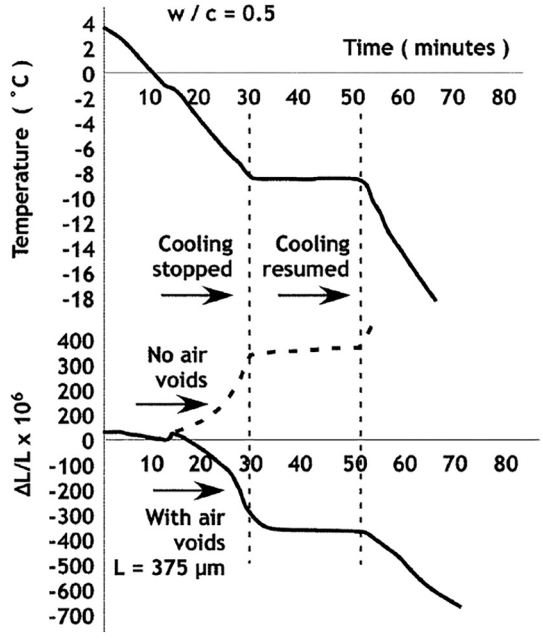

Fig. 3. Powers and Helmuth (1953) observed the length change (ΔL/L) evolution of two concrete samples with a water-cement weight ratio (w/c) of 0.5 for a certain temperature program of the climatic chamber (T) of 70 min. In one concrete mixture, an air-entraining agent was added to create a concrete with air void spacing (L) of 375 µm. A very different length change behaviour is noticed between the air-entrained concrete (solid ΔL/L curve) and the concrete without air voids (dashed ΔL/L curve) (after Scherer and Valenza, 2005).

The most feasible explanation for damage due to FT is founded on ability of a crystal to push particles. Already halfway the 19th century, Lavalle (1853) provided experimental evidence for pressure caused by crystal growth. He observed crystals being pushed upward, as precipitation of matter occurred at their bottom surface. Fifty years later, experiments by Becker and Day (1905) showed that an alum crystal has the ability to lift a substantial weight. To facilitate growth at loaded surfaces of a crystal, it is necessary to have a liquid film between the constraint and the crystal (Becker and Day, 1916; Correns and Steinborn, 1939; Taber, 1916). The existence of this liquid layer was proven by Gilpin (1979) and, for pure water, its thickness is estimated to approximately 0.9 nm (Brun et al., 1977).

Taber (1929, 1930) demonstrated that frost heave in soils also occurs with liquids that do not undergo a volume increase while solidifying, such as benzene, which counteracted the theory of volume expansion being the damaging mechanism in soils. Instead, he proposed the formation of **ice lenses** at the freezing front, which is fed with water from the capillary fringe below the freezing front. The thermodynamic theory behind **ice segregation** was further developed in soil research by Everett (1961). The theoretical pressures ice lenses and wedges in soils could generate were then quantified in the work of Miller (1972) and Gilpin (1980). Presently, the mechanisms for frost heave and ice segregation are rather well understood and several soil scientists have summarized and reviewed theories and models recently (Groenevelt and Grant, 2013; Peppin and Style, 2013; Rempel, 2010, 2012).

Similar experiments with benzene as Taber (1930) were performed on concrete and led to similar observations as for soils (Beaudoin and MacInnis, 1974; Litvan, 1978). This similarity made Walder and Hallet (1985) base their theory on crack widening of rocks by FT action on the ice segregation theory developed for soils. Eventually, Scherer (1993) used the same thermodynamical approach to explain pressure development during freezing in cement paste. Due to the analogy with damage done by salt crystal growth in porous media, the ability of a crystal to push particles is mostly referred to as **crystallization pressures** (Flatt et al., 2007; Scherer, 1999; Steiger, 2005a, 2005b).

3.2. Nucleation and ice growth in pores

The circumstances under which water will freeze are linked to the thermodynamic conditions. If the temperature drops below the melting point, it is thermodynamically more stable to crystallize. However, without the occurrence of nucleation, liquid will remain in a metastable state and this is referred to as supercooling. The interfacial free energy between the metastable liquid and solid state forms an energy barrier that prevents crystallization (Scherer, 1999). This barrier is overcome when a cluster of tens to hundreds of molecules forms by molecular movements in the liquid. If the cluster size has passed a critical size that overcomes the Gibbs free energy, the cluster is called a nucleus and will eventually evolve into a crystallite. Molecular clusters smaller than the energetic threshold, will dissociate again (Kalikmanov, 2013). This phenomenon is referred to as the Gibbs-Thomson effect (De Yoreo and Vekilov, 2003). During nucleation and growth of ice crystals the energy that is freed by the phase change is translated into latent heat release. Homogeneous nucleation causes the liquid to overcome the energy barrier spontaneously, which happens for pure liquid water at approximately −42 °C (Debenedetti, 2003; Sellberg et al., 2014).

Within porous geomaterials, however, crystallization is observed at much higher temperatures than −42 °C. Heterogeneous nucleation is triggered by ions, dust particles and interaction with topological surface impurities, such as cracks and pits. These are locations that all have a relatively low interfacial energy between the crystal and the solid pore wall (γ_{CS}). Young's equation links the interfacial energies of the different phases present through (Adamson and Gast, 1997):

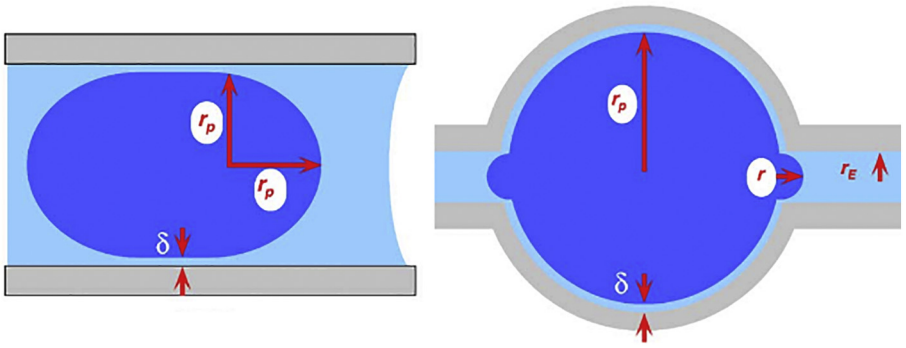

Fig. 4. Left: Image of an ice crystal (dark blue) surrounded by water (light blue) in a cylindrical pore with radius $r_p + \delta$ and the mineral pore walls in grey. The curvature at the end is given by κ_{CL}^{E} while the curvature at the cylindrical part is given by κ_{CL}^{S} (from Scherer (2004)). Right: A large pore with radius r_p with two small entries (radius $r_E + \delta$). As ice tries to intrude the small entries, the curvature of the intruding ice crystal is a lot more significant than the curvature of the ice in the large pore. Therefore, the largest pressure is found in the entrances of these small pores (from Scherer (2004)). (For interpretation of the references to colour in this figure legend, the reader is referred to the web version of this article.)

$$\gamma_{CS} = \gamma_{LS} - \gamma_{CL}\cos\theta \quad (1)$$

with γ_{LS} the interfacial energy between the liquid and the pore wall, γ_{CL} the interfacial energy between the ice crystal and the liquid and θ the contact angle between a crystal and the pore wall. Following Eq. (1), a favourable nucleation spot (minimal γ_{CS}) requires a small θ ($< 90°$). Most of the pore walls typically have a θ exceeding 90°, which causes crystal nucleation and growth to experience resistance (Scherer, 1999).

As small crystallites experience a capillary pressure as a result of their interfacial free energy, their melting temperature T is decreased according to the Gibbs-Thomson equation (Scherer, 1993, 1999):

$$T = T_m - \frac{\gamma_{CL} K_{CL}}{\Delta S_{fv}} \quad (2)$$

where T_m is the melting point of a bulk ice crystal ($\approx$273.15 K), γ_{CL} is the crystal/liquid interfacial free energy ($\approx$0.0409 J m^{-2}), ΔS_{fv} is the molar entropy of fusion ($\approx$1.2 J cm^{-3} K^{-1}) and K_{CL} is the curvature of the crystal-liquid interface and is defined by the principle radii of curvature $\frac{1}{r_1} + \frac{1}{r_2}$. For spherical crystals ($r_1 = r_2$) with radii of 67 and 33 nm, the melting point is reduced by 1 and 2 °C respectively (Scherer, 1999). Hence, for these small crystals, a higher supercooling is required to stabilize them (Scherer, 1993). Additionally, since the surface to volume ratio is very high for small crystallites, it is energetically more favourable to grow larger crystals. The relatively large crystallites will therefore win the competition on behalf of the smaller ones and they will grow accordingly. Under equilibrium conditions at a given temperature, all crystals have the same interface curvature K_{CL} (Scherer, 1999). Once nucleation has occurred, an ice crystal grows rapidly. At −1 °C the growth rate is 1600 μm/s (Hillig and Turnbull, 1956) and a water-filled pore of 200 μm would hence be filled with ice in approximately 0.12 s (Scherer and Valenza, 2005).

A water film with thickness δ ($\approx$0.9 nm) exists between the ice crystal and the pore wall (Gilpin, 1979; Webber et al., 2007), as a result of repulsive forces (or disjoining pressure) between both solid phases (Israelachvili, 2011). Hence, a pore-filling crystal with radius r_c relates to the pore radius r_p by $r_p = r_c + \delta$. Water can migrate through this surface film via diffusion over a characteristic time $t_e \approx x2/D$, with x the distance between two points and D the diffusion coefficient, which is estimated to be 10^{-11}–10^{-12} m^2/s in such water films (Scherer, 2006). For crystal growth into cylindrical pores, the curvature of the ice/liquid interface is written as:

$$K_{CL} = -\frac{2\cos\theta}{r_p} \quad (3)$$

With the existence of a water film between the ice and the pore wall, the contact angle (θ) is approximately 180°, which reduces K_{CL} to $-2/r_p$. Thus, from [2] and [3], the conditions for the penetration of a cylindrical pore can then be defined as:

$$r_p \geq \delta + \frac{2\gamma_{CL}}{\Delta T\, \Delta S_{fv}} \quad (4)$$

With ΔT the freezing point depression $T - T_m$.

3.3. Crystallization pressure

The liquid layer sustains itself by disjoining van der Waals forces between the crystal and the pore wall with a magnitude of several tens of MPa (Israelachvili, 2011). Hence, water can flow to the crystals, which secures growing possibilities. To prevent a crystal from growing larger than the pore, the pore wall must counterpart the pressures transmitted through the liquid layer. These are often referred to as **crystallization pressures** (Scherer, 1999).

In addition to a liquid layer, a constant flow towards the crystal is needed to continue growth. In other words, the liquid layer has to attract water molecules that are hydraulically connected. Everett (1961) found that it is energetically more favourable to grow crystals in the larger pores of the system first, while water in the smaller pores remains in a supercooled liquid state. Hence, at a certain temperature below the freezing point, a reservoir of unfrozen water is available and able to feed growing crystals in larger pores.

The tensile stresses caused by crystallization pressure can be quantified using a thermodynamical approach on a single crystal in a cylindrical pore (Fig. 4). The outer ends of a crystal growing in a cylindrical pore have a curvature $\kappa_{CL}^{E} = 2/(r_p - \delta)$, while curvature of the cylindrical side part of the crystal is given by $\kappa_{CL}^{S} = 1/(r_p - \delta)$. As the temperature is the same on all sides, both the top and the confined cylindrical side will try to grow. To prevent growth of the cylindrical side, additional pressure is provided by the pore wall (P_A) (Scherer, 2004):

$$P_A = \gamma_{CL}(\kappa_{CL}^{E} - \kappa_{CL}^{S}) = \frac{\gamma_{CL}}{(r_p - \delta)} \quad (5)$$

Maximal pressure occurs in large pores with small entries (Fig. 4). When a crystal grows in a pore with r_p with small entry radii ($r_E < < r_p$), the curvature of the ice in the large pore is almost flat compared to the curvature at the pore throat. This way, $\kappa_{CL}^{S} \approx 0$ and, hence the pressure only depends on the high curvature of the crystal in pore entry (κ_{CL}^{E}) ((Scherer, 2004).

$$P_A \approx \gamma_{CL}\kappa_{CL}^{E} = \frac{2\gamma_{CL}}{(r_p - \delta)} \quad (6)$$

In a cylindrical pore, the total crystallization pressure (P_C) exerted on the pore walls will be a tensile hoop stress written as:

$$P_C = \frac{P_A}{2} \approx \frac{\gamma_{CL}}{(r_p - \delta)} \quad (7)$$

During thermodynamic equilibrium, the curvature and energy of the crystal-liquid and liquid-vapour interfaces relate as $\gamma_{CL}K_{CL}^{E} = -\gamma_{LV}K_{LV}$ (Everett, 1961; Scherer, 1993). Since, for water, $\gamma_{CL} < \gamma_{LV}$, the curvatures relate as $K_{CL}^{E} > K_{LV}$. Therefore, an ice crystal nucleated within a water-filled pore is not able to drain water from a cylindrical neighbouring pore. In contrast, when the

temperature is low enough, it is the water that draws the ice into the cylindrical pore. Through balancing of the menisci, ice is however able to drain a tapered pore with the narrow end towards the crystal (Scherer and Valenza, 2005).

The pressure in the pore water (P_L) under thermodynamical equilibrium is given by (Scherer, 1999):

$$P_L - P_e = -\frac{2\gamma_{CL}}{(r_p - \delta)} \tag{8}$$

With P_e the equilibrium vapour pressure. Hence, in these conditions, crystallization pressure (P_C) cannot overcome the negative capillary pore pressure. For this reason, the net pressure is negative and contraction noticed when the length of a freezing sample is monitored (Scherer, 1999; Scherer and Valenza, 2005). Nevertheless, despite a net compression, a subject can degrade locally after many FT cycles, by means of fatigue (Sun and Scherer, 2010a).

Crystallization pressure can overcome the negative capillary pressures when the **thermodynamical equilibria** are interrupted. This can occur by two different processes. When the temperature has reduced sufficiently for ice to penetrate a certain water-filled pore, a water/air meniscus at the opposite side of a cylindrical pore is flattened by the sudden push caused by the 9% volume increase. The meniscus can return to an equilibrium curvature by evaporation of the excess water, however, the speed of the evaporation process is slow compared to the percolation speed of ice in the pore. Consequently, capillary pressure will not be able to keep up with the crystallization pressure and expansion will be noticed (Scherer and Valenza, 2005). However, for crystallization pressures to reach the mega-pascal range necessary for damage, ice penetration in pores smaller than 100 nm is required (Scherer, 2006).

A second disequilibrium can be reached by the strive of a crystal to have a uniform chemical potential everywhere in the crystal. When the temperature decreases and the ice crystal tends to grow, some areas of the crystal need to dissolve to liberate water for crystal growth elsewhere on the crystal surface. This water will be transported through diffusion in the nanometre-sized liquid layer between the crystal and the pore wall. If the transport proceeds too slow compared to the cooling rate, transient stresses could exceed the tensile strength of the material (Scherer, 2006). For ice crystals that are about 10 μm, the transport only takes a couple of minutes and, hence, transient pressures are rare for pores in this size range. In contrast, for ice crystals exceeding 1 mm diameter, the diffusion process could take over a day. Therefore, transient pressures are likely present in natural stones with relatively large pores (Scherer, 2006).

3.4. Cryosuction

Frost heave of soil and bedrock is facilitated by water flow towards growing ice lenses, referred to as cryosuction, a phenomenon which has been explained and quantified by Everett (1961). The basic explanation for cryosuction, also referred to as the capillary theory (Peppin and Style, 2013) is given by a shortened version of the Clausius-Clapeyron equation:

$$P_c - P_l = \frac{\rho_l L_f}{T_m}(T_m - T) \tag{9}$$

With P_c the ice pressure, P_l the water pressure, ρ_l the density of water, L_f the latent heat of fusion of ice at the bulk freezing temperature T_m and atmospheric pressure and T the temperature of the system. When a thermal gradient is applied on a porous water-bearing material, starting from sub-zero temperatures, an ice front will progress until it encounters a temperature under which it cannot further penetrate the pores in the system (Eq. (4)). The water below the ice front will remain in an unfrozen state and will act as a water reservoir. If the ice pressure is kept constant, for example when growth of the ice lens is resisted by pore walls or overburden pressure, the liquid pressure in the unfrozen reservoir needs to rise to maintain equilibrium (Eq. (9)). This pressure difference between ice and unfrozen reservoir water drives the latter towards the ice, where it will crystallize onto the forming ice lenses. The pressure that the ice lens exerts on the porous material is also defined by the crystallization pressure and follows Eq. (6).

The capillary theory could however not explain all experimental results. Peppin and Style (2013) define three problems with this model. First, the predicted maximum frost heave pressures deviated from experimental values for soils containing a range of particle sizes. Secondly, the Clapeyron equation fails when the system is outside an equilibrium. To solve the latter issue, a kinetic term was added to the Clapeyron equation (Style and Peppin, 2012). A third hiatus in the capillary theory is the inability the explain the growth of new, intermittent ice lenses. For this, frozen-fringe models have been developed (e.g. Miller, 1972; Rempel et al., 2004). Here, frozen fringe refers to a partially frozen zone that might allow slow unfrozen water movement. A frozen fringe below a growing ice lens provides nuclei where new ice lenses could potentially grow. Despite frozen fringes are likely to be present in freezing rocks (Hallet et al., 1991; Walder and Hallet, 1985), their presence in soils is highly debated. There are models that predict intermittent ice lens growth without the presence of a frozen fringe, i.e. the engulfment model (Asthana and Tewari, 1993; Mutou et al., 1998) and the geometrical supercooling mode (Style et al., 2011). The current thermodynamical theories on water movement during freezing, (intermittent) ice lens formation and frost heave have been comprehensively reviewed recently by several authors (e.g. Groenevelt and Grant, 2013; Peppin and Style, 2013; Rempel, 2010, 2012).

3.5. From pressure to damage

Once the total pressure generated by the generation of ice crystals or ice lenses overcomes the local tensile strength of the frozen material, damage will be generated. The tensile stress generated in a single pore can overcome the tensile strength of the material by the processes described above. However, only if a volume comparable to the stress-controlling flaws of the material is subjected to pressures, fractures can be induced. Scherer (1999) argues that damage occurs when the temperature has dropped sufficiently low to enable ice growth in pores with a breakthrough pore radius (r_{bt}), which corresponds to the characteristic pore size that controls the liquid permeability. This pore-size is estimated from the inflection point of a cumulative pore-size distribution (Katz and Thompson, 1986). As the ability to enter a pore of a certain size is linked to the temperature, a corresponding breakthrough temperature (ΔT_{bt}) can be defined based on Eq. (4):

$$\Delta T_{bt} = \frac{2\gamma_{cl}}{(r_{bt} - \delta)\Delta s_{fv}} \tag{10}$$

Once ΔT_{bt} is reached and ice can percolate through the pore space, a stress field is created large enough to possibly overcome the strength of the material (Scherer, 1999).

The larger the concentration of ice in a specific volume, the more likely pore walls will be affected by crystallization pressure and the risk of failure is increased. The ice crystal saturation degree (S_C), defined as the molar percentage of water transformed into ice crystals, can be estimated at a certain temperature using scanning calorimetry (Johannesson, 2010), AC impedance spectroscopy (Perron and Beaudoin, 2002) or a dielectric capacitive apparatus (Fabbri et al., 2006). S_C can also be determined via a theoretical approach based on thermodynamics (Coussy and Monteiro, 2007).

Poromechanics, a branch in mechanics that combines poroelasticity (Biot, 1941) with continuum thermodynamics, allows us to upscale stress calculated in a single pore to stress in a volume of porous solid, filled with air, water and ice. An extensive overview on poromechanics is given by Coussy (2004); its application for salt and ice crystallization

in pores is described by Coussy and Monteiro (2007). The tensile stress over a volume is linked to S_C and the crystallization pressure on the pore walls. So to determine the tensile stress, the crystallization pressure over the entire volume (ΔP_C) needs to be known and is given by (Coussy, 2006):

$$\Delta P_C = \frac{3K\varepsilon_f}{\beta_p S_C} \tag{11}$$

Wherein ε_f is the linear strain, K is the bulk modulus for a dry sample and β_p the Biot coefficient for poroelastic expansion of the material, for which $\beta_p = 1 - K/K_m$ with K_m the bulk modulus of the solid phase. An approximation for the macroscopic stress (σ) on a larger volume is described by Espinosa-Marzal et al. (2011) as follows:

$$\sigma \approx \beta_p S_C P_C \tag{12}$$

To cause fractures within the material of interest, the equation below is necessarily fulfilled (Coussy, 2006; Espinosa-Marzal et al., 2011):

$$\sigma > \frac{\sigma_t}{\sqrt{3(1-2\nu)}} \tag{13}$$

With σ_t is the tensile strength measured in a uniaxial tensile strength test and ν the Poisson's ratio of the material. The tensile strength is mainly important within cemented materials, such as rocks and building materials. In the framework of frost heaving, where the medium lacks a rigid skeleton, it is overburden pressure due to the weight of the matter above the ice front that is necessarily surmounted by the crystallization pressures (Gilpin, 1980; Miller, 1972).

It should be emphasised that failure can arise in two possible manners. Either the damage is immediate by pressures exceeding the tensile strength of the material, or the material fails by the accumulation of stresses over time. These two ways of failure are referred to as critical and sub-critical failure respectively and are discussed below in this order.

In several publications, Fagerlund (1975, 1977, 2004)) stated that a fully frost resistant porous brittle material does not exist. From experiments on concrete, he concluded that every material has a certain critical water saturation above which **critical failure** occurs when exposed to negative temperatures. Below the critical saturation level, no damage should occur, while from the critical saturation level onward, the residual strain is linearly correlated to the saturation degree (Fig. 5). The influence of the moisture saturation on frost resistance was also investigated for natural building stones by several authors (e.g. Chen et al., 2004; Prick, 1997), confirming the critical saturation concept for critical failure. Rocks with a moisture level exceeding the critical saturation therefore tend to increase in porosity, decrease in E modulus or show a residual strain after a single FT cycle. Repeated FT cycles do not seem to have an influence on the critical moisture content of concrete. However, once the critical water level has been exceeded,

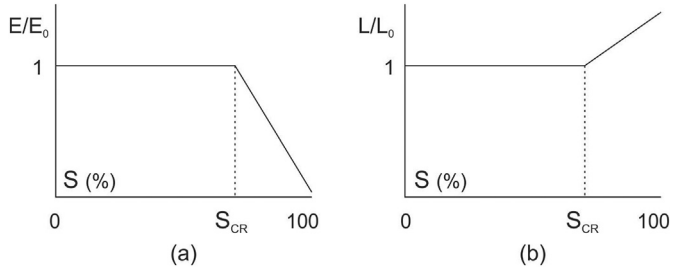

Fig. 5. The critical saturation degree S_{CR} can be measured by (a) determining the dynamic *E*-modulus before (E_0) and after (E) a FT cycle or (b) determining length before (L_0) and after a FT cycle. Before S_{CR} is reached, there will be no change in E or L after a cycle, while after the S_{CR} threshold value, E will decrease and L will increase linearly with the degree of saturation (S).

the residual strain after following FT cycles is proportional to the water content of the sample during these FT cycles (Fagerlund, 2004).

Materials with a moisture content lower than the critical saturation level also tend to lose strength over time due to exposure to sequential FT cycling. Hence, damage is induced by stresses which do not exceed the strength of the material. This phenomenon is often referred to as **sub-critical crack growth** (e.g. Chau and Shao, 2006; Ishikawa et al., 2004; Kemeny, 1991; Nicholson and Nicholson, 2000) or fatigue cracking (Griggs, 1936; Hall, 1999). For rather frost resistant materials, over one thousand FT laboratory simulations need to be performed before any damage through fatigue is observed (Ruedrich et al., 2011). Many well recognized and hypothesised chemical and physical processes are known to act at a crack tip to assure subcritical crack growth. However, most of those theories are poorly understood and strongly debated. The most common explanation for geological materials is weakening of the lattice around a stressed pre-existing flaw tip by chemical interactions with the pore water (Atkinson, 1980, 1984). If crystallization pressure or any other stress mechanism is subsequently applied, cracks tend to grow more easily. In a recent review on the mechanics of subcritical cracking, Eppes and Keanini (2017) argue that climate-dependent subcritical cracking is potentially the process responsible for most crack growth in surface and near-surface rocks. In the long term, this process is thus equally important as the critical damage discussed before. Moreover, by long-term exposure to a certain climate, the parameters for critical damage might alter due to the build-up of subcritical damage in the structure.

3.6. Damage location and evolution

Nicholson and Nicholson (2000) established that pre-existing rock-strength flaws, such as sedimentary bedding planes, elongated fossils and micro-cracks are also preferentially activated during FT simulations on building stones. Just below the surface, these rock strength flaws are often grain boundaries and hence, granular disintegration is often attributed to FT cycles. The initially formed microscopical cracks are invisible for the human eye. During subsequent FT cycles after crack initiation, ice will preferentially nucleate within the crack, causing it to widen. In geomorphology, this widening of existing cracks is referred to as frost wedging rather than frost cracking. Microscopic observations with μCT, also revealed the growth of a micro-crack by an microscopic ice lens or wedge (De Kock et al., 2015). The crack was formed by the presence of a pre-existing flaw and opened progressively more during freezing stages, while it closed again upon thawing. After a certain number of cycles, the fracture remained open during thawing, but did not grow larger upon freezing. This demonstrated the influence of a fixed moisture content during the experiment, as after a certain number of FT cycles, enough accommodation is created for the ice to grow unconfined. From the moment water is added to the system, crack growth by frost wedging will continue.

Continuous FT cycling is able to induce progressively more micro-cracks in the matrix of a material. Once a critical number of these micro-cracks coalesce, damage will progress rapidly over a short amount of FT cycles, causing a non-linear decay (Martinez-Martinez et al., 2013). When this process occurs in the outer layer of a stone, loss grains, flakes or scales can be observed consequently. The micro-crack growth rate depends mainly on the mechanical properties of the material. For example, granites will not weather fast by FT action if at all, whereas e.g. certain porous limestones will.

On a larger scale, frost heave is observed in soils and bedrock as ice lenses form parallel to the freezing front, with resulting cracks also having that orientation (Murton et al., 2006). Bedrock outcrops often have many joints caused by phenomena other than FT weathering, e.g. exhumation, tectonic or isostatic movements, thermal cycling, biological growth or lithological variations. In low permeable rocks, these joints control most of the water storage and transport and, upon freezing, ice lenses will thus preferentially form here. Therefore,

similarly as for frost heave, these existing cracks will also propagate through frost wedging, although in a direction depending on the local mechanical situation.

4. Assessment of FT weathering

Several aspects of FT weathering are investigated both in laboratory and field conditions. General FT weathering tests performed by (geo-) engineers mostly evaluates the FT susceptibility of a material. However, many investigators attempted to find the boundary conditions of material and climatological variables to explain the observed FT damage. Based on the fit with the observations, theoretical explanations for FT damage were developed, adapted or dismissed. Eventually, models arose which attempt to predict the occurrence of pore-scale and large scale damage.

4.1. Laboratory methods

4.1.1. Steady state evaluation

In general, frost resistance of a certain material is assessed in laboratory by the study of structural changes induced by simulating the weathering conditions on samples. Material samples are cyclically loaded under specified normalised protocols, after which the changes in the rock properties are determined. These tests are static, or steady state, since they only reflect the resulting damage and not the actual damaging process. Usually, to investigate the macroscopic damage, **visual observations** of the changes are made first. As damage results in an increase in porosity and/or weakening of the subject, several methods are often employed to assess the characteristics prior to and after a number of FT cycles. Most common are the determination of **weight**, and measuring **porosity** and apparent density through water absorption (e.g. Martins et al., 2016). Often, the **pore-size distribution** is found through mercury intrusion porosimetry (MIP) (Abell et al., 1999; Diamond, 2000). **Strength** parameters are often determined non-destructively by measuring the propagation of acoustic waves through the material through an ultrasonic pulse velocity test (Feng et al., 2019; McAllister et al., 2013; Prick, 1997) or by a Schmidt hammer test (Yavuz, 2011; Yavuz et al., 2006) or destructively by a compressive (Martinez-Martinez et al., 2013), flexural (Sun et al., 1999) or tensile strength test (Al-Omari et al., 2015). The evolution of porosity and internal structure has also been measured by using nuclear magnetic resonance (NMR) (Li et al., 2018). **Imaging techniques**, such as optical microscopy and scanning electron microscopy, are also employed to visualise and evaluate internal structural changes prior to and after FT cycles (Jacobsen et al., 1995).

FT damage has also been evaluated and quantified using **X-ray computed tomography** (CT) (de Argandoña et al., 1999) and X-ray micro-computed tomography (μCT) for natural stone (Cnudde and Boone, 2013; Dewanckele et al., 2013), mortar (Promentilla and Sugiyama, 2010) and concrete (Suzuki et al., 2010). A benefit of this technique is its non-destructive nature and the ability to image an object in 3D. Hence, 3D micrometre scale assessments of the internal damage evolution caused by FT cycles were performed (Fig. 6).

Since all porous building materials have a different weathering behaviour, and the environment also varies with geography, many **FT laboratory simulations** have been developed locally for specific mineral building materials. Therefore, it is hard to compare results for FT resistivity obtained from different standards. To generalise the results, international standards have been developed (e.g. European standard tests EN 12371 for natural stone, CEN/TS 772-22 for clay masonry and CEN/TS 12390-9 for concrete). Other widely used standardised tests are developed by the American Society for Testing and Materials (e.g. ASTM D5312/D5312M for natural stones, ASTM C67/C67M – 18 for bricks and ASTM C1645 – 16 for concrete). Despite the usefulness of these standard test methods, many tests are still performed using local standards or are adapted to better suit the experiment. Therefore, the differences between the standards still causes a disability to compare results.

The European standardised FT cycle for natural building stones (EN 12371) takes 12 h in the climatic chamber with a specific temperature evolution. For economic reasons, these tests are mostly limited to only a couple dozen cycles. During such tests, most deterioration is related to the main rock discontinuities, such as pre-existing fractures, heterogeneities or sedimentary bedding (Nicholson and Nicholson, 2000; Thomachot and Jeannette, 2002). For this reason, the results of these laboratory tests mainly focus on these flaws, whereas the importance of total fabric decay is often neglected. Long-term FT cycling carried out by Ruedrich et al. (2011) pointed out that rapid (50 cycles) tests only give limited information on the real FT susceptibility of a stone. In some cases, about 1400 cycles are necessary to provide an in-depth assessment of the frost susceptibility.

Results of accelerated FT weathering tests are then compared to the performance of the material of subject in the field (Al-Omari et al., 2015; McAllister et al., 2013; Thomachot et al., 2005). A comparative study by McGreevy and Whalley (1985) revealed that the moisture content reached within rocks during laboratory simulations are hardly found in natural conditions. Hence, they raised awareness that weathering simulations could induce exaggerative effects or could display unnatural weathering behaviour. Comparison of results of accelerated cycles in lab and observations in the field often show discrepancies (Ingham, 2005). This raises questions on the integrity of the laboratory tests, and the influence of other weathering processes under atmospheric and laboratory environment (McAllister et al., 2013).

4.1.2. Dynamic monitoring

Apart from the overall frost susceptibility of a certain material, results from static tests are not explanatory on how water redistributes, damage initiates, cracks grow or stop growing. To gain insight in the damaging mechanisms rather the process than the effects should be monitored. For that purpose, proxies that reflect the water-ice phase transition can be used with appropriate monitoring methods.

One of the most natural proxies to determine ice crystallization is the **temperature** of the cooling system. Crystallization of water is an exothermal process caused by the production and diffusion of latent heat of fusion. In temperature measurements, this will be translated into a heat spike or exotherm (Hall, 1988, 2004, 2007). The properties of this exotherm (i.e. intensity, duration) are related to the amount of water that crystallizes. It will approximate 0 °C (or the equilibrium melting temperature T_m according to the crystal curvatures, given by Eqs. (2) and (4)), and, depending on the amount of water that is able to freeze, the exotherm will remain stable at that temperature (Fig. 7). This phenomenon is called the zero-curtain effect (Outcalt et al., 1990).

The smaller a pore, the lower the temperature necessary to freeze the water inside it (Scherer, 1999). As the pore space of building materials mostly consists of a range of pore sizes, multiple exothermal peaks can appear as the temperature drops, indicating multiple crystallization phases (Kaufmann, 2004) (Fig. 8). This defines also the base of thermoporometry (Brun et al., 1977; Landry, 2005). By the use of a thermal scanning calorimeter (DSC), the exothermal peaks of freezing, the endothermal peaks of melting and the hysteresis between those two curves enable to derive the pore-size distribution and other pore characteristics (i.e. connectivity and shape) of the material (Sun and Scherer, 2010b). With this technique, also the ice content can be estimated (Johannesson, 2010; Koniorczyk and Konca, 2017).

With temperature, the dimensions of a material will change following its linear thermal expansion coefficient. However, when pore water is present, capillary and crystallization pressures are generated in situ as the water freezes, changing the **strain pattern** of the material (Fig. 7). The growth of ice tends to expand the ice-bearing material. However, (cryo-)suction of water from smaller pores generates negative pressures that counteract the expansive forces of the ice, leading to a complex length change pattern (Powers and Helmuth, 1953).

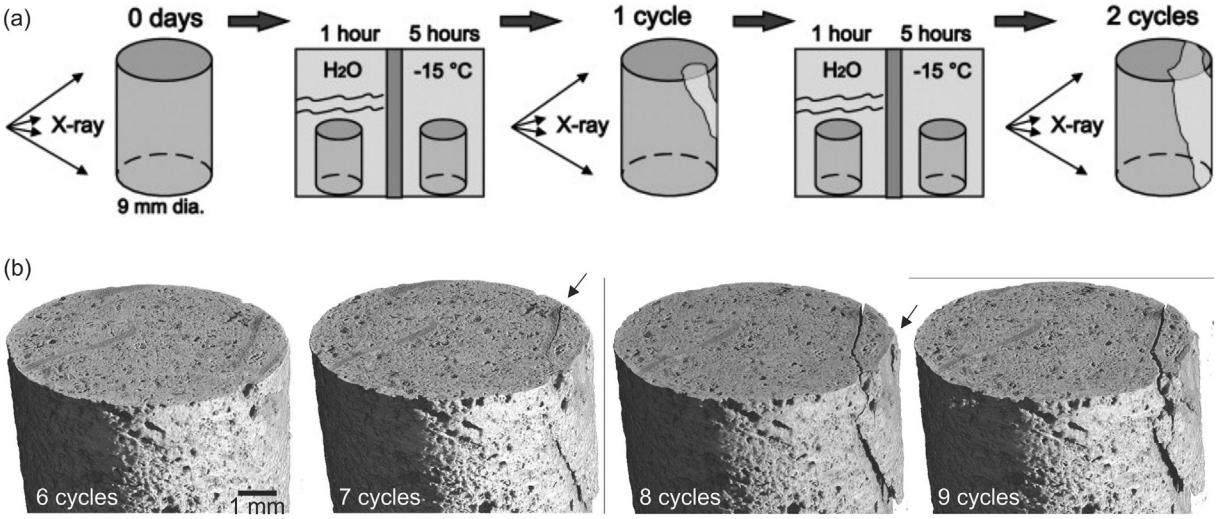

Fig. 6. (a) Methodology to evaluate FT weathering by use of μCT. A 9 mm diameter core sample is first imaged and subsequently subjected to the first FT cycle which consists of 1 h of saturating in water and 5 h of freezing followed by thawing and drying. The sample is then imaged again to visualise and measure the changes in the structure. This can be repeated several times. (b) Results of the workflow described in (a) after 6 to 9 FT cycles performed on a Noyant limestone drilled core. Cracks become visible after 7 cycles and tend to develop along a certain fossil (from Dewanckele et al., 2013).

Additionally, the coefficient of thermal expansion of cement paste, concrete, limestone or sandstone (Table 1) is significantly smaller than the coefficient of ice. Hence, when cooled together, ice crystals shrink faster than the solid structure surrounding them, influencing the net strain of the frozen material (Kaufmann, 2004; Ruedrich and Siegesmund, 2007; Sun and Scherer, 2010a).

By monitoring the length changes during FT cycle and varying parameters such as the saturation degree or the cooling rate, an assessment can be made on the flow behaviour of the water (Prick, 1995). Development of sufficient pressure during the cycle, results in a residual strain. This means that the volume of the sample has increased, indicating that additional pore space has been formed. A damage estimation can thus be derived from these observations. Several authors performed similar experiments to have a more in-depth analysis on the frost resistivity or to verify their models for processes occurring in the pore system (e.g. Kaufmann, 2004; Powers and Helmuth, 1953; Prick, 1997; Ruedrich and Siegesmund, 2007; Sun and Scherer, 2008; Thomachot-Schneider et al., 2018; Thomachot and Matsuoka, 2007).

Events of crack initiation and growth will generate sound waves, often referred to as acoustic emissions. These can then be captured by attaching microphones to the material. Evidently, monitoring the number of incoming waves over time with decreasing temperature leads to an assessment of the internal damage (Hallet et al., 1991; Shimada et al., 1991; Todak et al., 2017; Verstrynge et al., 2018). The more counts the microphones detect, the more cracks have appeared or grown. These observations can be linked with results of a length change test, as most of the counts coincide with a phase of expansion (Kaufmann, 2004). Moreover, when the same event is detected by multiple receivers, it can be traced to the location of the newly appeared or growing crack (Duca et al., 2014). The more receivers that

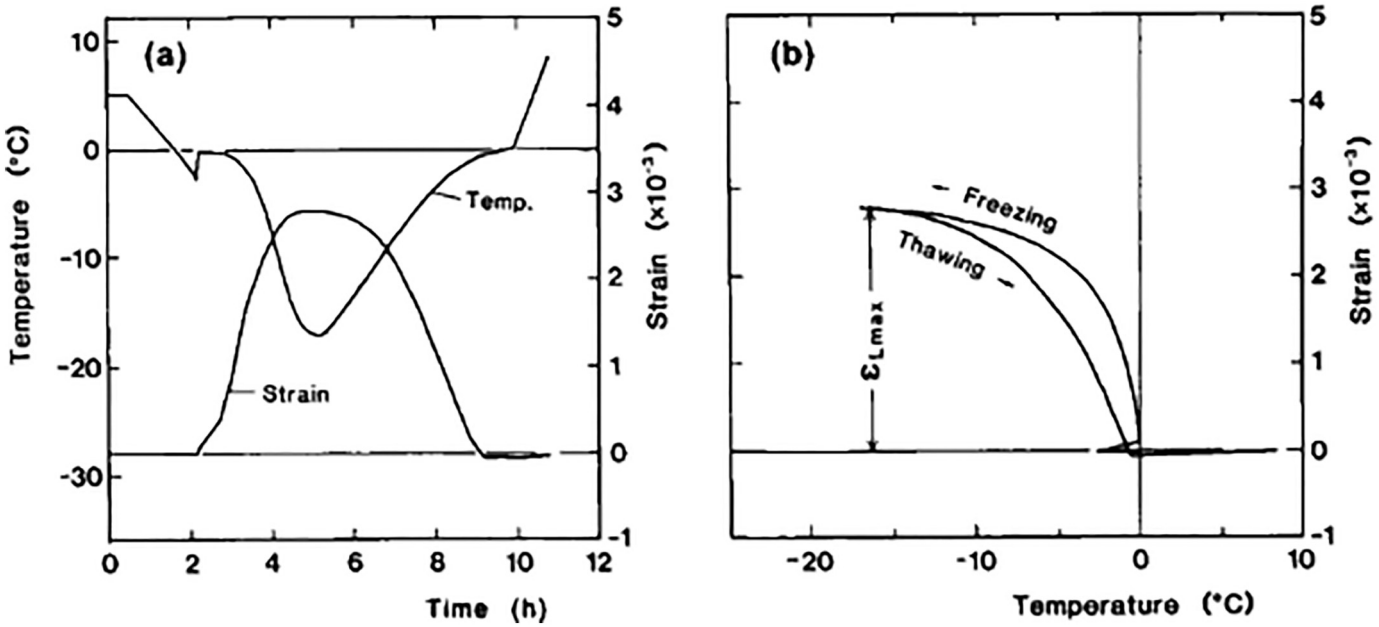

Fig. 7. In situ temperature and length evolution of a tuff exposed to a single FT cycle. (a) Temporal evolution of rock temperature (with a zero curtain) and strain and (b) strain linked to rock temperature (from Matsuoka, 1990a).

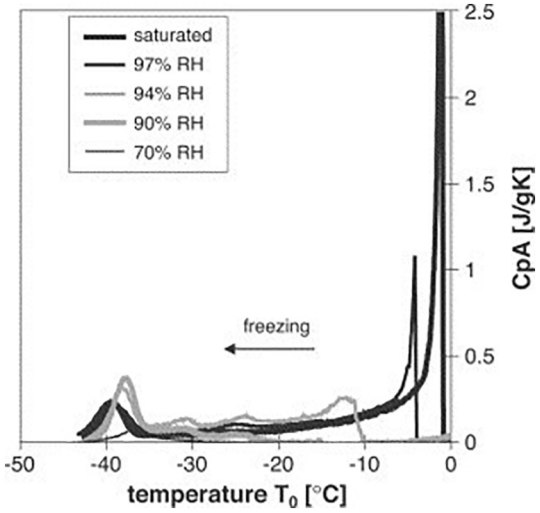

Fig. 8. Peaks in the apparent heat capacity (CpA) of concrete in function of the negative temperatures can be linked to the pore sizes in which water resides. Different peaks arise in function of the water saturation degree (relative humidity (RH)) (from Kaufmann (2004)).

Table 1
Linear expansion coefficients for ice and several porous building materials.

Material	Linear expansion coefficient (10^{-6} / K)
Ice	50 (Butkovich, 1957)
Cement paste	15–20 (Meyers, 1951)
Concrete	8–12 (Uygunoglu and Topcu, 2009)
Limestone	4–6 (Steiger et al., 2014)
Sandstone	9–12 (Steiger et al., 2014)

are placed around the sample, the more accurate the crack can be located three-dimensionally (Schubert, 2004).

Next to monitoring passively the sounds created by the object, actively sending **ultrasonic pulses** through an object delivers valuable information on its structure. As mentioned before, this non-destructive method is used to determine strength parameters in a static manner. It is however also possible to measure the acoustic properties during a freezing process. Through this method, the amount of ice formed in the pores can be quantified. When pore water freezes, the acoustic velocity increases significantly. Hence, the measured wave transit time between a transducer and a receiver can indicate the amount of frozen water, following:

$$t_u - t_f = V_i\left(\frac{1}{c_w} - \frac{1}{c_i}\right) \tag{14}$$

where t_u and t_f are the unfrozen and frozen transit time respectively. c_w and c_i are the sound velocities in water and ice respectively and V_i is the volume of ice. Hence, the volume of ice can be estimated for different temperatures of cooling (Kaufmann, 2004).

Additionally, measuring the changes in **dielectric constants** can be of added value to attempt to quantify the amount of ice (Fabbri et al., 2009). The same counts for **neutron diffraction** (Swainson and Schulson, 2001), as the ice peaks appear in the diffraction patterns while freezing. When calibrated, these peaks can be translated in an amount of frozen water. To determine the relation between supercooling and the pore size in which crystallization occurs, the **nuclear magnetic resonance** relaxation time has proven its worthiness (Jehng et al., 1996; Prado et al., 1998). When all ice is frozen, no response occurs as all molecules are fixed in a crystal lattice. As soon as thawing occurs, the relaxation time prolongs in function of the pore size wherein water has occurred. By making relaxation time profiles over different temperatures, one can follow the pore-sizes that are freed from ice when thawed.

Although **scanning electron microscope** observations are considered static, this imaging technique can be performed on frozen samples as a cryogenic environment can be created around the sample. Although this still eliminates the ability to do fully dynamic experiments, there is the ability to 'flash-freeze' the sample at any point in time during a FT cycle. Imaging 'flash-frozen' samples, enables us to assess the position of growing crystals at very high resolution. The morphology of ice crystals in pores was investigated with this technique on cement paste samples (Corr et al., 2004; Corr et al., 2002) (Fig. 9) Figure 9:. After the ice was imaged, the temperature was raised, which caused the crystals to sublimate, and the region of interest was imaged again. Hence, a clear ice signature could be derived from the images.

μCT was mentioned as a stationary method to assess the damage caused by FT cycles. Recent developments in laboratory μCT have enabled researchers to produce full 3D volumes in less than 18 s (Bultreys et al., 2015). Hence, processes with a temporal resolution lower than a minute, can be imaged in high quality. By implementing a custom-made freezing cell onto a μCT device, De Kock et al. (2015) were able to image a freezing process of a limestone both dynamic and in vivo. Through this method, the researchers were able to visualise and quantify the initiation and growth of cracks during freezing and subsequent closing of the cracks during thawing (Fig. 10).

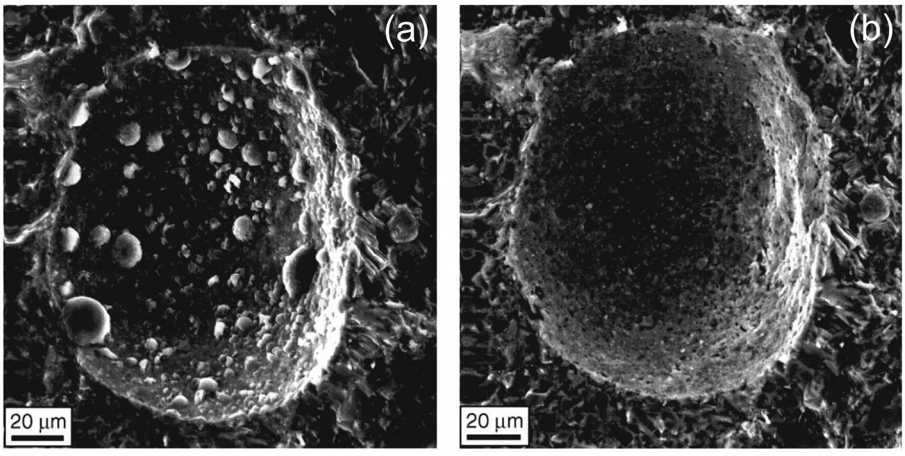

Fig. 9. (a) An air void in a water-saturated cement paste that has been flash frozen and (b) after the ice has been sublimated. Comparing (a) and (b) indicates that the crystals seen in (a) are indeed multiple ice crystals and that they seem to form at pore throats where capillary pores enter the air void (from Corr et al., 2004).

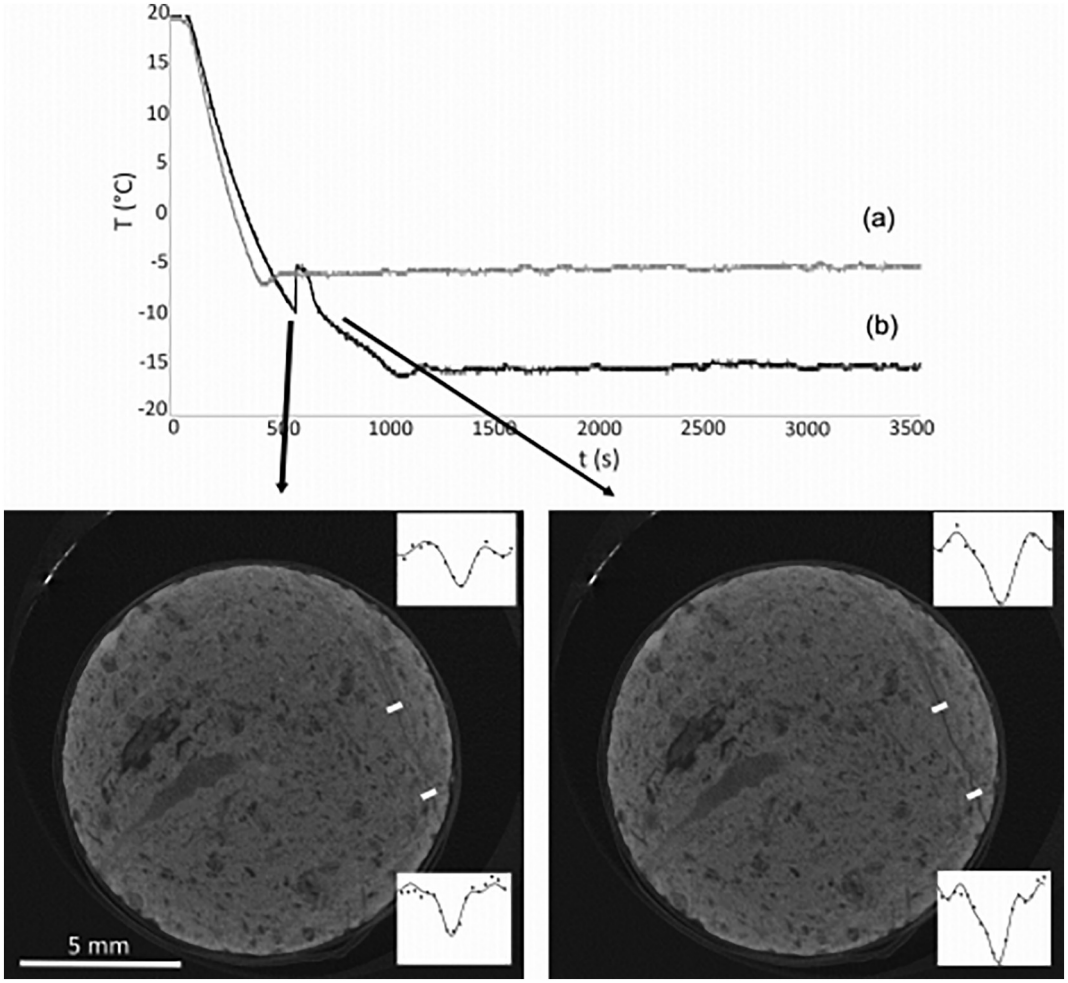

Fig. 10. The temperature evolution of a Noyant limestone during a freezing experiment with minimal temperatures of −5 °C (a) and − 15 °C (b). An exothermal event, coupled to the initiation of ice crystallization, is only noticed when a sample reaches −9.7 °C. This temperature can be linked to a specific pore size present in the stone. Continuous μCT scanning then revealed that this exotherm coincides with the opening of a crack. The crack width is shown in the insets in the corners of the μCT images (from De Kock et al., 2015).

4.2. Field methods

Field investigations mostly focus on bedrock and soil in periglacial and mountainous areas and cultural heritage sites. Field monitoring of concrete structures with emphasis on FT weathering is mostly limited to visual observations of a cracked surface (e.g. Li et al., 2012). Geo-scientists often seek to define the boundary conditions for damage or debris generation by frost wedging or heaving. Therefore, the applied techniques are often twofold, with techniques focussing on the damage on the one hand and climatological parameters on the other hand. Only then, the climatological triggers for damage can be interpreted correctly (Draebing et al., 2017; Eppes et al., 2016; Matsuoka, 2019; Matsuoka and Sakai, 1999; Phillips et al., 2016). Hence, methods to measure heat and moisture distribution are discussed next, before proceeding to methods that cover damage quantification.

Some of the following techniques are mobile and/or larger variants of previously described lab-based techniques. Anyhow, for calibration of these methods, laboratory measurements are often necessary. When considering bedrock or soils, both destructive and non-destructive methods are employed, while for built structures, non-destructive measuring techniques are preferred. The latter could however limit the internal information of the investigated subject compared to an equivalent destructive technique.

4.2.1. Heat and moisture distribution

In situ temperature data is mostly gathered by placing temperature sensors on well-considered places on or within the rock (e.g. Anderson, 1998; Gruber et al., 2004; Hall, 1998; Hall and André, 2001; Hasler et al., 2011; Matsuoka, 1994). When multiple sensors are applied over a certain time period, a spatial and temporal temperature distribution can be made for the area and/or subsurface of interest. In mountainous regions, the temperature conditions within the subsurface has been measured in boreholes, which allows to reconstruct the permafrost temperature in the deeper subsurface (Luetschg et al., 2004; Schneider et al., 2012). On cultural heritage, non-destructive methods are mostly preferred, limiting the ability to determine inner temperatures. Surface temperatures are normally monitored by contact sensors or infrared radiometers (Camuffo, 1998). Besides measuring temperature, infrared thermography has also been applied to detect moisture (Avdelidis and Moropoulou, 2004; Avdelidis et al., 2003; Moropoulou et al., 2013) and damage in built infrastructures (Aggelis et al., 2010; Kordatos et al., 2013).

Hall (1986) discussed that **water content** is a crucial factor to frost weathering of bedrock. Hence, to understand the weathering behaviour, this parameter should be monitored both temporally and spatially. A combination of several methods is required to arrive at a reasonable approximation of the real water content through space and time (Sass, 2005a) and therefore, determining water content and distribution is a difficult and time-consuming task. The same counts for

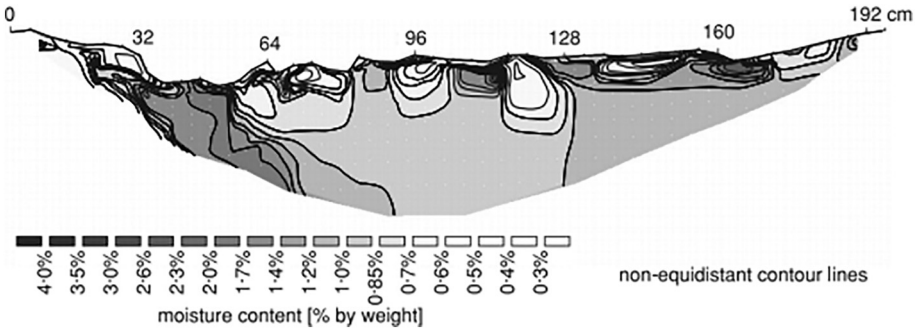

Fig. 11. An example of a moisture content spatial 2D distribution (in % by weight) over a transect of 192 cm long resulting from the ERT technique. The maximal penetration depth here is 0.4 m (from Sass, 2005a).

monitoring water distribution in built walls (Snethlage and Wendler, 1997). Sass and Viles (2006) stated that many methods are available, however, calibrating the obtained data and cross-checking between results of different sources was proven difficult.

Direct determination of moisture content is done by analysing the weight of hammered samples or drill powders using carbid meters or gravimetrical methods before and after drying (Sandrolini and Franzoni, 2006; Sass, 2005a). Novel handhold sensors are based on microwave propagation (Orr et al., 2019a, 2019b). Another technique is measuring the humidity by placing moisture-sensitive sensors in a drilled hole within the material. Most of these sensors measure the electrical resistivity, since this parameter varies with the water content. However, the resistivity is also influenced by the temperature and therefore, these point measurements can be inaccurate. This can be solved by applying a thermo-moisture probe (e.g. Matsuoka, 2019). Time domain reflectometry (TDR) involves measurement of the speed of propagation of an electrical pulse between two electrodes, which is directly correlated to the water content (Sass, 2005a). When more electrodes are applied on a transect, there is the ability to map the moisture content in 2D over that line profile (Fig. 11). This method is referred to as electrical resistivity tomography (ERT) (Hauck, 2002). To obtain moisture data out of the resistivity data, calibration of the moisture/resistivity curve in the lab is needed (Hassine et al., 2018; Sass, 2005a). If ERT is applied regularly on the same transect, a time dimension is added to the moisture distribution. Hence, it enables to monitor temporal variations of the moisture distribution. The technique has been widely applied on soils (Samouëlian et al., 2005; Schwartz et al., 2008), rock (Mol and Viles, 2010; Sass, 2005a) and on building materials and cultural heritage (Hassine et al., 2018; Orr et al., 2016; Sass and Viles, 2006, 2010).

Besides water, also ice is detected by the ERT method (Sass, 2004), which allows the method to be applied for permafrost research (Isaksen et al., 2011; Krautblatter and Hauck, 2007; Watanabe et al., 2012). An overview of other geo-electrical methods applicable for permafrost research, such as ground penetrating radar (GPR) (Steelman et al., 2010), capacitive resistivity imaging (CRI) (Kuras et al., 2011) is found in Kneisel et al. (2008).

4.2.2. Observing damage

FT weathering is mostly expressed by widening of existing cracks and by generation of debris. Therefore, the detection of displacement is crucial here. Many of the measuring campaigns mentioned here stretch over several years, to have sufficient displacement data in many different climatological conditions. An overview of techniques used in the field to quantify bedrock weathering is given by Krautblatter and Dikau (2007).

Rocks that have broken off a rock wall can be caught in a collector net (Krautblatter and Moser, 2009; Vehling et al., 2019) or a natural rock trap (Vehling et al., 2016). The volume of this debris results in an estimation of a rockwall retreat. Frequently emptying the collectors allowed researchers to observe increased rockfall events at certain time periods. Additionally, time lapse camera monitoring (Matsuoka, 2019) or time lapse laser scanning (Abellán et al., 2014; Strunden et al., 2015), attribute to the identification and quantification of rockfall activity. The dimensions of the caught debris, reveal information on the depth or extent of activated fractures. After analysing the debris generated at a several rock walls for 12 years, Matsuoka (2008) attributed relatively small debris to short-term FT cycles, while the occurrence of relatively large boulders was observed more during thawing of the seasonal ice in spring.

One drawback to this method is however the time lag between the cracking, or the weathering event, and the detachment. Small to intermediate-grained pieces of rock are often gathered in so-called intermediate storage sites along the slope (Müller et al., 2014; Sass and Krautblatter, 2007). Events in which these stored rocks are transported down-slope are called secondary rockfalls (Luckman, 1976). Secondary rock fall events can contribute a substantial amount of the total collected rock volume (Krautblatter and Moser, 2009). However, by registering the fallen rock volume on a daily basis, the origin of the rockfall can be related to the meteorological circumstances. Moreover, rock collectors can be installed at multiple spots that are particularly sensitive to different kinds of rockfall events to assess the impact of both primary and secondary rockfalls (Krautblatter and Moser, 2009). Also the dimensions of the collector, or a sieving maze on top of it, help to differentiate between rockfall sources (Sass, 2005b). Large secondary rockfalls are typically frequent during or after intense rainfall events, while periods of freeze-thaw cycling barely cause additional secondary rockfalls (Krautblatter et al., 2006; Krautblatter and Moser, 2009; Sass, 2005b).

The opening and closing of a fracture in bedrock can provide information on the growth of an ice wedge within it. This process can be measured by use of **displacement sensors** such as crackmeters or extensometers (Blikra and Christiansen, 2014; Draebing et al., 2017; Hasler et al., 2012; Ishikawa et al., 2004; Matsuoka, 2001a, 2008), devices similar to strain gauges used on a smaller scale. Frost heave has been monitored with vertical extensometers on soils (Matsuoka et al., 1997; Watanabe et al., 2012) and horizontal displacement transducers on brick walls (Thomachot et al., 2005). Many of these observations reveal short-term and seasonal events. In several studies, Matsuoka and co-authors revealed limited crack widening due to diurnal FT cycles in autumn, while in spring, important crack widening is attributed to refreezing of meltwater within cracks (Matsuoka et al., 1997; Matsuoka, 2001a, 2008).

Acoustic techniques have also been adapted to perform field measurements. Actively measuring the ultrasonic pulse velocity through walls is a common technique to determine the overall damage done to the structure (Moropoulou et al., 2013). Moreover, it has been used to measure the moisture content and its evolution (Hall, 1997). Acoustic emission (AE) monitoring has also been performed to detect periods of intensive cracking correlated with FT events in the field

(Amitrano et al., 2012; Girard et al., 2013a). The acoustic emission technique however limits to acoustic events occurring in the upper meter below the subsurface. Fracturing of bedrock that occurs deeper has been monitored with micro-seismicity (MS) technique (Amitrano et al., 2005, 2010; Weber et al., 2018). The difference between AE and MS, and also the reason for the depth dependency, lies in the frequency range of the measured waves. AE waves lie the higher sonic to ultrasonic frequency spectrum (10^4–10^6 Hz), while MS waves have a frequency in the lower sonic to infrasonic spectrum ($1-10^3$). High frequency waves are attenuated more by the intersected solid phases, which makes the AE technique unfit to detect events at larger depths.

4.3. Freeze-thaw indexation

To estimate the potential of FT induced damage, **frost indices** are frequently used. These try to couple complex physical processes to comprehensive numbers to ease the assessment of potential damage (Grossi et al., 2007). The first kind of indices are based on climatological variations. The simplest index is the number of yearly FT cycles, determined by monitoring the air temperature over a certain period. This index does however not include moisture availability, which is necessary for FT weathering to occur. A combination of the temperature and the latter is given by the yearly wet FT cycles, which counts days of heavy rain immediately followed by negative temperatures (Grossi et al., 2007). Other indices are linked immediately to physical damage. Based on the theoretical work of Walder and Hallet (1985), several researchers state that fractures will only grow when the temperature lies within the 'frost cracking window' (Anderson, 1998; Hallet et al., 1991; Walder and Hallet, 1985) ranging from −3 to −8 °C for most rocks. This frost cracking window was used to develop predictive models for the frost cracking of bedrock due to ice segregation, together with mean annual temperatures and the temperature gradient within the rocks (Andersen et al., 2015; Anderson, 1998; Hales and Roering, 2007). Recently, damage isopleths have been developed for different kinds of bricks. These indicate the risk for damage based on the moisture content and the minimal temperature (Feng et al., 2019).

A combination of observations on temperature and moisture distribution both in lab and field, led to enough data to develop hygrothermal **simulation software** such as WUFI (Künzel, 1995) and Delphin (Nicolai et al., 2007). Petrophysical properties of the material and the climatological conditions are used as input. These software packages are then able to simulate the moisture, vapour and heat flux through the material or a wall assembly. This approach was developed first in building physics (Sedlbauer and Künzel, 2000) and is of special interest for cases of retrofitted walls, but recently it also found its way to earth sciences (Rode et al., 2016). FT risk assessment is mainly based on arbitrary pass/fail criteria such as the occurrence of a critical moisture content in combination with a specific temperature drop (Calle and Van Den Bossche, 2017; Straube et al., 2010; Zhou et al., 2017).

Additionally, numerical algorithms to simulate the actual frost-induced pressure have been developed since the beginning of the 21st century (Hain and Wriggers, 2008; Koniorczyk et al., 2015; Kruschwitz and Bluhm, 2005; Liu et al., 2011, 2014; Wardeh and Perrin, 2008; Zuber and Marchand, 2000). For the development of numerical models, several assumptions need to be made on e.g. damage theories, critical thresholds and material properties. Therefore, every model has some discrepancies when compared to actual experimental data. However, as the knowledge on the pressure mechanisms has evolved, computer simulations have become more elaborate and accurate. Nowadays, researchers are working on upscaling the pore-scale models into modelling of entire structures (Eriksson et al., 2018).

5. Discussion

5.1. Parameters influencing FT weathering behaviour

Concluding from previous theoretical sections, several parameters determine the appearance of frost induced damage. It mostly incorporates the pore characteristics of the cooling subject, the available water content, the cooling rate, the duration and the minimal temperatures reached. Often these parameters are closely related to each other resulting in complex interactions.

5.1.1. Pore characteristics and saturation

First, the pore characteristics and pore-size distribution regulate potentially stored water amount. With an increased amount of initial pore water, the resulting pressures after crystallizing are potentially larger too. Secondly, the pore-size distribution also defines how much water will crystallize at certain negative temperatures and how much pressure will be generated by this process. The critical saturation level is therefore inevitably entwined with the pore characteristics of a material.

In unfrozen state, water is stored throughout the pores based on the capillary forces, which are in turn determined by the pore size (Hall and Hoff, 2002). Since the smallest pores exhibit the largest capillary pressures but the lowest absorption velocity, small pores will fill the slowest but will eventually drain larger pores. This process will halt when an equilibrium state is reached in function of the capillary pressure of the system. When additional water enters the system, progressively larger pores will saturate over time as the capillary pressure decreases.

This equilibrium concept enables to link water saturation S_L to the pore-size distribution. When sub-zero temperatures are applied on this system, the conditions for the penetration of a pore [Eq. (4)] determine the link between the pore-size distribution and temperature. Consequently, S_L can be defined for a certain degree of supercooling ΔT. $S_L/\Delta T$-graphs provide material-specific insight in S_L and the crystal saturation degree S_C, which is defined as $1 - S_L$, at a fixed temperature of supercooling. This was demonstrated by Coussy and Monteiro (2008) on samples of mortars with different pore-size distributions (Fig. 12). In soil sciences, the link between the moisture distribution, or soil water curve (SWC), and the temperature and ice content, or soil freezing curve (SFC), has also been extensively studied to use in mathematical models on moisture and heat transport. A recent review of these models is given by Kurylyk and Watanabe (2013).

To estimate the crystallization pressure in a larger volume, Eq. (9) is required. A length change experiment could then provide ε_f and since S_C can be estimated based on the $S_L/\Delta T$-graphs, ΔP_C can be linked to the ice content, the temperature of the system and the pores that are penetrated.

A certain stressed volume is needed to translate the crystallization pressures into damage. The theory on a 'breakthrough temperature' and consequent 'breakthrough pore radius' was already established in a previous section (Eq. (8)) (Scherer and Valenza, 2005). On the one hand, materials with a relatively large breakthrough radius will be prone to stress at less negative temperatures. On the other hand, the crystallization pressures are lower in large pores (Scherer, 1999). Frost resistance of a certain material will hence be dependent on the volume and size range of stressed pores.

Better frost resistance was found for natural building stones with unimodal and focussed pore-size distributions (Ruedrich et al., 2011; Ruedrich and Siegesmund, 2007). The authors attributed this to the lack of a supercooled reservoir and the ability to freeze most of the water at once. Within natural building stones, the amount of pores with a size between 10 and 0.1 μm is important for damage by crystallization (Benavente, 2011). The presence of pore throats with a size between 0.1 and 1 μm was later correlated with enhanced FT weathering (Martinez-Martinez et al., 2013). Ink-bottle pores present in oolithic limestone

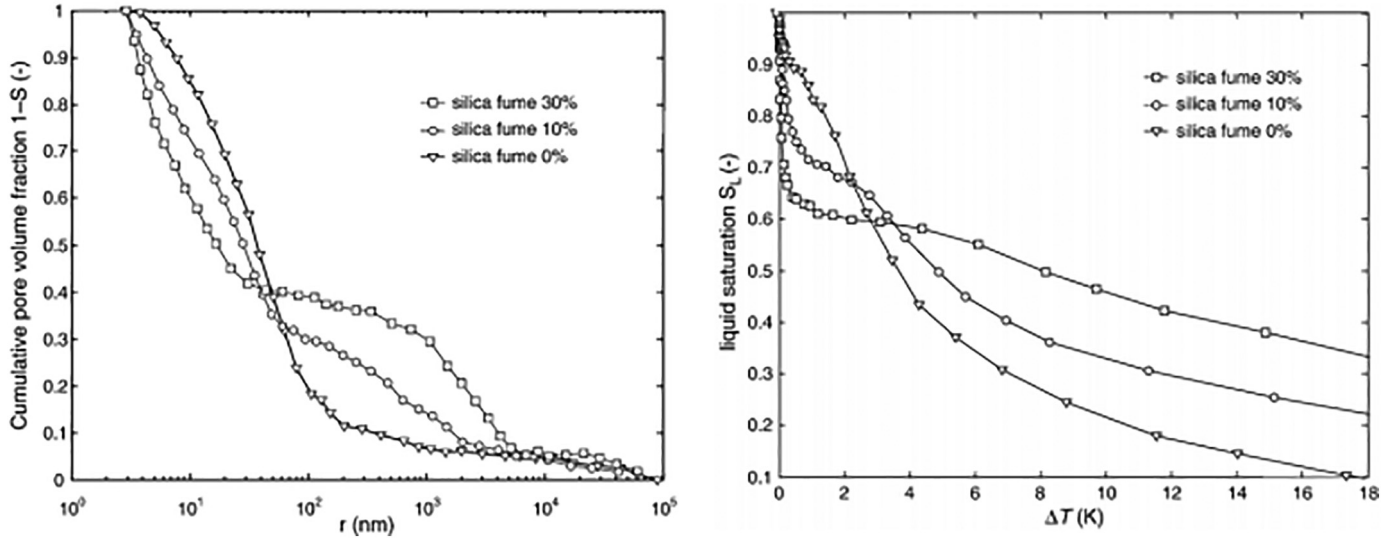

Fig. 12. On the left some cumulative pore-size (r) distributions of three mortars with each a different silica fume content. This component is a byproduct of the silicon industry and used as an additive in cement for its highly reactive pozzolan character. On the right the liquid saturation S_L in function of temperature ΔT derived from the pore-size distributions on the left and Eq. (4). The ice crystal content can be calculated at every point as $S_C = 1 - S_L$ (from Coussy and Monteiro, 2008).

mitigate the effect of FT weathering as these pores act as an expansion reservoir (Deprez et al., 2020). The same process has also been observed in cementitious materials that contain air voids (Sun and Scherer, 2010a). These fairly large pores are able to drain the water from the neighboring much smaller pores upon freezing. That water subsequently freezes within these large ink-bottle pores or air voids, in which the crystals will grow unconstrained. This process reduces the risk of high crystallization pressures occurring in small pores.

Also on a larger scale, the influence of the water availability and porosity on the FT weathering patterns was described by many authors. Enhanced frost shattering has been found in places that stimulate a high rock moisture content, such as river or lake shores (Blikra and Longva, 1995; Matthews et al., 1986). Weathering is also enhanced when negative temperatures are preceded by rainfall or snow events that increase the moisture content (Matsuoka, 2019). Melting of a snowcover in spring and subsequent refreezing causes widening of cracks (Matsuoka, 2001a). Porous bedrock weathers faster through ice segregation during diurnal FT cycles due to fast transport of water to ice lenses (Akagawa and Fukuda, 1991; Matsuoka, 2001a). In contrary, in solid bedrock, ice segregation fractures manifests themselves deeper within after a longer period under constant sub-zero temperatures, providing sufficient time for water migration to the freezing front (Matsuoka, 2001a; Walder and Hallet, 1985) These conditions occur within the seasonal frost layer (Hallet et al., 1991; Murton et al., 2000) or at the top of the permafrost layer (Murton, 1996; Murton et al., 2000).

5.1.2. Temperature and time

It should be remarked that not all episodes of negative temperatures result in ice formation (Hall, 2007). If temperatures do not extend far enough below the freezing point, water could remain in the supercooled state. This could be the case if only a limited amount of water is present in the host material. However, in natural open environments, in which cracks, ions, dust particles, snow crystals, lichens, etc. will act as nucleation spots, supercooling prior to nucleation is mostly not observed (Matsuoka, 2001b).

Time and temperature are directly linked to the depth of freezing. Matsuoka and Murton (2008) divided FT events in three categories based on their duration and intensity. High frequency short-term (diurnal) FT events lead to only shallow freezing. Seasonal FT cycles cause freezing up to several meters depth. The last category, long-term FT events occur from climate change and will not be further discussed here.

The built environment is mostly exposed to the first category of FT cycles. Unidirectional freezing from the surface causes inwards propagation of a freezing front. Subsequently, water migration from the unfrozen inner part to the freezing front contributes to the formation of ice lenses at a certain depth below the surface. This specific formation depth mostly relies on the applied thermal gradient, which in turn depends on the thermal properties of the rock, the atmospheric pressure and the water content. Damage caused by these diurnal FT cycles is limited to the upper millimetres to decimetres of the material. Additionally, an increasing number consecutive FT cycles obviously rises the risk of fatigue failure. Matsuoka, 2001b argued that with an increasing number of FT cycles, more water accumulates in superficial areas within the subject. Over a larger period of time, for instance a single winter, the surficial layer can potentially reach the critical saturation threshold locally.

Besides the diurnal FT cycles, soils and bedrock in periglacial and mountainous areas are prone to seasonal FT cycles. During winter, longer periods of negative temperatures can be reached which favour the growth of ice lenses at depths up to several meters. A longer cold period would extend the time for cryosuction towards the freezing front, causing also cracking in rather impermeable rocks. Especially materials connected to a permanent water reservoir at low capillary pressures are more prone to such situation, which is exactly what happens at heaving soils where the ice lens is in contact with the capillary fringe (Peppin and Style, 2013).

However, the presence of a permafrost layer causes a different temperature profile and thus a different weathering behaviour. Only the active layer is prone to seasonal changes, while the permafrost layer remains frozen. Therefore, during melting of the active layer in summer, disequilibria causes downward cryosuction of the meltwater and ice lenses form at the top of the frozen permafrost layer, which results in frost heave (Murton et al., 2000, 2006). Refreezing meltwater in cracks also caused increased frost wedging during seasonal thaw (Girard et al., 2013b; Matsuoka, 2008). Moreover, seasonal thaw has been linked to increased boulder fall at steep slopes (Matsuoka and Sakai, 1999).

Walder and Hallet (1985), theoretically defined a ‘frost cracking window’ (Anderson, 1998), which is a temperature range in which cracks tend to grow, based on the fracture toughness of the frozen material and the size of a pre-existing crack. The existence of this temperature range was verified in the lab by several authors (Akagawa

and Fukuda, 1991; Hallet et al., 1991; Murton et al., 2000) and a window between −3 and − 8 °C is often used to predict enhanced cracking (Hales and Roering, 2007). This window however varies with the porosity, pore-size distribution, water content, the presence of initial cracks and tensile strength and therefore, this window should be defined per material (Matsuoka, 2001b).

A slow cooling rate enhances water transport and ice lens growth (Powers and Helmuth, 1953). A fast cooling rate should then promote fast growth into the smallest pores of the system and fast percolation of ice through the structure. In simulations on marbles and granites, the cracks grow larger with decreasing cooling rate for a fixed target temperature, while with a fixed period of cooling, cracks tended to grow only when an intermediate cooling rate (0.1 °C/h) was applied (Walder and Hallet, 1985). These authors argued that for a higher cooling rate (0.2 °C/h), water freezes fast in the smaller pores, shutting off the pathways towards a possible ice lens. For lower cooling rates (0.025 °C/h), the authors discuss that the thermodynamic disequilibrium is built up slowly, also causing limited flow towards growing ice lenses.

Experiments on the effects of the cooling rate on the length change behaviour of closed porous system (no water is added or removed) was done by several authors (e.g. (Blachere and Young, 1972; Litvan, 1972; Matsuoka, 1990b). Similar as the results of Walder and Hallet (1985), the lowest cooling rate did not display much stress. Here, researchers attributed this to the slow pressure build-up and the ability of ice to deform or 'creep' (Matsuoka, 1990b). Ruedrich and Siegesmund (2007) argued that stress, built up by crystallization pressure, can be released by pressure solution of the ice crystals once supercooled water is depleted from the pore space.

5.1.3. Scale

As frost weathering is a multi-disciplinary topic, geologists, geomorphologists, physicists, soil scientists and engineers each have developed theories on how the pressure builds up and damages their material of interest (Hall and Thorn, 2011). Geo-scientists are often confronted with features on a very large scale, as they are looking to landscape evolution. In the field, results of frost weathering are mainly identified as mechanically weathered blocks, rock falls or heave of soils. Therefore, their questions concerning weathering are mainly answered by a large-scale approach on the subject, for which frost heave and frost wedging is explained by the ice segregation theory.

However, Hall (2004) pointed out that different ways of degradation can result from the same weathering phenomenon and that scale should not play a role in this matter. Hence, in case of FT weathering, flaking or the loss of grains is probably caused by the same process that widens fissures and loosens bedrock on a larger scale. De Kock et al. (2015) demonstrated that cracks form by ice segregation in pre-existing flaws and that frost wedging gradually widens the crack on a microscopical scale. This is largely the same process as seen in large fractured bedrock in the field. Therefore, differentiation between microgelivation and macrogelivation (Matsuoka, 2001b) is based on the resulting scale of damage rather than the process.

5.2. Future approaches in FT weathering research

From previous sections, it is clear that different parameters need to be investigated to assess the FT weathering behaviour. Material and environmental variables are complex and numerous and, moreover, climate change will shift the latter both temporally and geographically. Despite numerous theoretical approaches, lab and field observations, the relation between all variables during a FT cycle is presently not fully resolved. This currently limits us from selecting more durable building materials, applying better measures and precautions to sensitive existing structures and predicting potential natural hazards, such as rock falls, in a more adequate fashion.

Investigating pore-scale processes is not that straight-forward. To understand the processes underpinning a FT cycle, the effect of every variable parameter on e.g. strain, temperate regime of the system or acoustic emissions should be examined more closely, both independently and in combination. Such task would ask to assume other factors to be constant during the experiment. The cooling rate, the minimal and maximal temperatures and the duration of a cycle can be kept constant during an experiment easily, while maintaining the saturation degree without considerably manipulating the experiment is more difficult. To prevent water gain or loss, the application of an impermeable coating is necessary. This coating can interfere with the normal crystallization pattern and insulate the samples, which causes uncertainties of the temperature regime. Additionally, before an experiment is started, the moisture distribution within the pores has to follow the capillary equilibrium so that it can be modelled using capillary pressures.

Many rocks are not homogeneous in material properties, which of course affects results of FT tests. Hence, it is hard to produce exact values for FT susceptibility. Moreover, nucleation is a stochastic process, meaning that parameters, such as the nucleation temperature and the ice volume formed during initial nucleation, are defined as probability functions based to other parameters such as the water content and the cooling rate. To derive these probabilities, a large number of measurements on different samples under different circumstances would be necessary. Of course, these tests would take a hideous amount of time and are consequently not executed.

Small samples offer some advantages towards the randomness of crystallization as they only contain a few favourable nucleation spots and only a very limited number of pre-existing flaws if any at all. The ability to focus on only a couple of nucleation spots, would be beneficial to elucidate the nucleation and crystal growth process, together with the following water redistribution. If many cycles would be performed on this millimetre-sized sample, fatigue could also appear. Hence, the temporal and spatial evolution of ice crystals and eventually the locations of damage initiation are important to determine on this small scale. Doing such experiments in function of all the variables would define and explain the critical boundaries and that be a giant step forward in understanding FT weathering on the small scale. Once the pore-scale processes are recognized from these small samples, the weathering behaviour on a larger building or outcrop scale can be better explained.

Despite the great added value of temperature and strain monitoring, these techniques measure merely proxies for the pore-scale processes and, therefore, they only provide limited insight in in-situ crystal growth and water redistribution. To improve the knowledge on the pore-scale, it is required to deliver direct proof. For this, methods that are able to visualise the pore space while a FT cycle is applied, should be further explored. These imaging techniques should have a temporal and spatial resolution sufficiently high to resolve all processes on the pore scale. Once suited techniques are established, the theories regarding FT weathering can be confirmed or reshaped.

The μCT technique delivers 3D volumes with resolution up to approximately 1 μm and has been extensively applied in geo-sciences over the last two decades (Cnudde and Boone, 2013). However, the technique also comes with some drawbacks. Many rocks and building materials have a large fraction of pores below the spatial resolution limit of laboratory μCT devices. Therefore, the pore space cannot be visualised entirely with the current state-of-the-art, although developments such as dark field imaging could offer opportunities for the future (Revol et al., 2011). Moreover, the X-ray attenuation of water and ice is similar, which implies that the two phases can hardly be distinguished based on X-ray attenuation when appearing in pores together. The maximal temporal resolution that is currently reached in laboratory μCT setups is 12 s per tomography (Dierick et al., 2014). For imaging the fracture evolution, this proved to be sufficient (De Kock et al., 2015). However, nucleation and crystal growth are processes that complete in a matter of seconds, too fast to be resolved by the temporal

resolution. Nonetheless, lab-based μCT remains a promising technique to further investigate crack growth under different conditions (Shields et al., 2018), redistribution of water during FT cycles (Deprez et al., 2017, 2020) and propagation of an ice front.

Synchrotron-based X-ray imaging techniques could offer a solution to certain shortages of laboratory-based X-ray techniques. The brightness of the synchrotron radiation enables very fast image acquisition, which reduces the time for a tomography to not even a second. This would resolve the temporal resolution issue of the lab-based systems. Multiple synchrotron beamlines are moreover able to reach higher spatial resolutions that the common lab-based μCT systems. Some synchrotron-based techniques offer promising applications towards the differentiation and visualization of water and ice in a porous medium. For example, the crystal lattice of ice diffracts the incoming X-rays, which causes the appearance of a phase contrast at the border between water and ice in X-ray tomograms. This technique was recently applied to identify frozen and unfrozen parts within food (Guo et al., 2018). Also the diffraction pattern of ice itself can be used to produce a three-dimensional image of the diffracting crystals (Ludwig et al., 2009). Although present applications are limited to metallurgic materials, applying a diffraction-based three-dimensional imaging technique could deliver a significant contribution to several aspects of the behaviour of ice in porous mineral materials.

Combining direct with indirect observations is the key to solve remaining frost-related questions. To validate a process observed with e.g. μCT, measurements of indirect properties linked to the water-ice phase transition are of major importance. De Kock et al. (2015), for example, demonstrated that a crack opened simultaneously with an exotherm in the temperature curve, which immediately proves that crystallization was the cause of the damage (Fig. 10). Within the same experiment, the exact temperature of the freezing point depression lead to an assessment of the pores in which nucleation occurred, resulting in an explanation for the location of initiated crack. Shields et al. (2018) combined μCT with AE monitoring and established that the water saturation degree was correlated with the size and location of the induced cracks. Building a set-up that is able to image while measuring a proxy in real-time is however not easy. For μCT, most systems have to rotate the sample for 360°, which hinders the use of attached cables for conditioning and measuring devices. Also, the larger the surrounding of the sample gets, the lower the resolution of the tomography will be due to magnification issues. Developing and incorporating a specific measuring and/or conditioning device into a μCT system is therefore always well-considered and system specific.

Future research should focus on developing and testing new techniques that can possibly deliver direct proof of the pore-space processes. Combining these techniques with existing methods for determining parameters related to FT weathering, will lead to a better understanding of the results coming from the latter. This combination will enable researchers to attribute weathering behaviour to one or multiple pressure build-up mechanisms in the pore space. By varying the environmental conditions of FT experiments, parameters for numerical modelling will be extracted. Existing numerical models can be enhanced consequently and prediction of the FT weathering behaviour of porous mineral materials will be more accurate.

As there a scale-independency in the weathering mechanisms, these developments on the pore-scale will also lead to better assessments of the large-scale implications of frost cracking and wedging within surface rocks or within built structures. To test the validity of these models on a large scale, more sites in frost-sensitive areas should be fully monitored for temperature and rock moisture content (Rode et al., 2016) and resulting FT damage patterns (acoustic emissions, crack opening). Here, both the spatial and temporal resolution of measurements is of key importance.

Declaration of Competing Interest

The authors assure that there is no conflict of interest.

Acknowledgments

This work was financed by Research Foundation Flanders (FWO), project 3.G.0041.15. Tim De Kock was a postdoctoral fellow supported by FWO and acknowledges its support. The authors wish to thank the three anonymous reviewers for their constructive comments on the manuscript.

References

Abell, A.B., Willis, K.L., Lange, D.A., 1999. Mercury Intrusion Porosimetry and image Analysis of Cement-based Materials. J. Colloid Interface Sci. 211, 39–44. https://doi.org/10.1006/JCIS.1998.5986.

Abellán, A., Oppikofer, T., Jaboyedoff, M., Rosser, N.J., Lim, M., Lato, M.J., 2014. Terrestrial laser scanning of rock slope instabilities. Earth Surf. Process. Landf. 39, 80–97. https://doi.org/10.1002/esp.3493.

Adamson, A.W., Gast, A.P., 1997. Physical Chemistry of Surfaces, 6th ed. Wiley.

Aggelis, D.G., Kordatos, E.Z., Soulioti, D.V., Matikas, T.E., 2010. Combined use of thermography and ultrasound for the characterization of subsurface cracks in concrete. Constr. Build. Mater. 24, 1888–1897. https://doi.org/10.1016/J.CONBUILDMAT.2010.04.014.

Akagawa, S., Fukuda, M., 1991. Frost heave mechanism in welded tuff. Permafr. Periglac. Process. 2, 301–309. https://doi.org/10.1002/ppp.3430020405.

Al-Omari, A., Beck, K., Török, Á., Brunetaud, X., Al-Mukhtar, M., 2015. Critical degree of saturation: a control factor of freeze-thaw damage of porous limestones at Castle of Chambord. France. Eng. Geol. 185, 71–80. https://doi.org/10.1016/j.enggeo.2014.11.018.

Amitrano, D., Grasso, J.R., Senfaute, G., 2005. Seismic precursory patterns before a cliff collapse and critical point phenomena. Geophys. Res. Lett. 32, 1–5. https://doi.org/10.1029/2004GL022270.

Amitrano, D., Arattano, M., Chiarle, M., Mortara, G., Occhiena, C., Pirulli, M., Scavia, C., 2010. Microseismic activity analysis for the study of the rupture mechanisms in unstable rock masses. Nat. Hazards Earth Syst. Sci. 10, 831–841. https://doi.org/10.5194/nhess-10-831-2010.

Amitrano, D., Gruber, S., Girard, L., 2012. Evidence of frost-cracking inferred from acoustic emissions in a high-alpine rock-wall. Earth Planet. Sci. Lett. 341–344, 86–93. https://doi.org/10.1016/J.EPSL.2012.06.014.

Andersen, J.L., Egholm, D.L., Knudsen, M.F., Jansen, J.D., Nielsen, S.B., 2015. The periglacial engine of mountain erosion-part 1: rates of frost cracking and frost creep. Earth Surf. Dyn. 3, 447–462. https://doi.org/10.5194/esurf-3-447-2015.

Anderson, R.S., 1998. Near-surface thermal Profiles in Alpine Bedrock: Implications for the Frost Weathering of Rock. Arct. Alp. Res. 30, 362–372.

Anderson, R.S., Anderson, S.P., Tucker, G.E., 2013. Rock damage and regolith transport by frost: an example of climate modulation of the geomorphology of the critical zone. Earth Surf. Process. Landf. 38, 299–316. https://doi.org/10.1002/esp.3330.

Asthana, R., Tewari, S.N., 1993. The engulfment of foreign particles by a freezing interface. J. Mater. Sci. https://doi.org/10.1007/BF00367810.

Atkinson, B.K., 1980. Stress corrosion and the rate-dependent tensile failure of a fine-grained quartz rock. Tectonophysics 65, 281–290.

Atkinson, B.K., 1984. Subcritical crack growth in geological materials. J. Geophys. Res. Solid Earth 89, 4077–4114. https://doi.org/10.1029/JB089iB06p04077.

Avdelidis, N., Moropoulou, A., 2004. Applications of infrared thermography for the investigation of historic structures. J. Cult. Herit. 5, 119–127. https://doi.org/10.1016/J.CULHER.2003.07.002.

Avdelidis, N.P., Moropoulou, A., Theoulakis, P., 2003. Detection of water deposits and movement in porous materials by infrared imaging. Infrared Phys. Technol. 44, 183–190. https://doi.org/10.1016/S1350-4495(02)00212-8.

Beaudoin, J.J., MacInnis, C., 1974. The mechanism of frost damage in hardened cement paste. Cem. Concr. Res. 4, 139–147. https://doi.org/10.1016/0008-8846(74)90128-8.

Becker, G.F., Day, A.L., 1905. The linear force of growing crystals. Proc. Washingt. Acad. Sci. 7 (0363–1095), 283.

Becker, G.F., Day, A.L., 1916. Note on the Linear Force of growing Crystals. J. Geol. 24, 313–333.

Benavente, D., 2011. Why pore size is important in the deterioration of porous stones used in the built heritage. Rev. la Soc. española Mineral. doi. https://doi.org/10.1007/s12665-010-0815-9.

Benavente, D., García del Cura, M.A., Fort, R., Ordóñez, S., 2004. Durability estimation of porous building stones from pore structure and strength. Eng. Geol. 74, 113–127. https://doi.org/10.1016/J.ENGGEO.2004.03.005.

Biot, M.A., 1941. General Theory of Three-Dimensional consolidation. J. Appl. Phys. I. Gen. theory Phys. Fluids J. Chem. Phys. J. Math. Phys. J. Chem. Phys 12. https://doi.org/10.1063/1.1676909.

Blachere, J.R., Young, J.E., 1972. The Freezing Point of Water in Porous Glass. J. Am. Ceram. Soc. 55, 306–308. https://doi.org/10.1111/j.1151-2916.1972.tb11291.x.

Blikra, L.H., Christiansen, H.H., 2014. A field-based model of permafrost-controlled rockslide deformation in northern Norway. Geomorphology 208, 34–49. https://doi.

org/10.1016/j.geomorph.2013.11.014.
Blikra, L.H., Longva, O., 1995. Frost-shattered debris facies of Younger Dryas age in the coastal sedimentary successions in western Norway: palaeoenvironmental implications. Palaeogeogr. Palaeoclimatol. Palaeoecol. 118, 89–110. https://doi.org/10.1016/0031-0182(94)00141-T.
Brun, M., Lallemand, A., Quinson, J.-F., Eyraud, C., 1977. A new method for the simultaneous determination of the size and shape of pores: the thermoporometry. Thermochim. Acta 21, 59–88. https://doi.org/10.1016/0040-6031(77)85122-8.
Bultreys, T., Boone, M.N., Boone, M.A., De Schryver, T., Masschaele, B., Van Hoorebeke, L., Cnudde, V., 2015. Fast laboratory-based micro-computed tomography for pore-scale research: Illustrative experiments and perspectives on the future. Adv. Water Resour. 8https://doi.org/10.1016/j.advwatres.2015.05.012. 55–1.
Butkovich R., T., 1957. Linear thermal expansion of ice. US Army Snow Ice and Permafrost Research Establishment, Corps of Engineers 40.
Calle, K., Van Den Bossche, N., 2017. Analysis of different frost indexes and their potential to assess frost based on HAM simulations. In: De Schutter, G., De Belie, N., Janssens, A., Van Den Bossche, N. (Eds.), 14th International Conference on Durability of Buildings Materials and Components. RILEM Publications S.A.R.L, Ghent, pp. 434.
Camuffo, D., 1998. Developments in Atmospheric Science 23: Microclimate for Cultural Heritage. Elsevier, Amsterdam.
Chatterji, S., 1999. Aspects of the freezing process in a porous material–water system: part 1. Freezing and the properties of water and ice. Cem. Concr. Res. 29, 627–630. https://doi.org/10.1016/S0008-8846(99)00035-6.
Chatterji, S., 2003. Freezing of air-entrained cement-based materials and specific actions of air-entraining agents. Cem. Concr. Compos. 25, 759–765. https://doi.org/10.1016/S0958-9465(02)00099-9.
Chatterji, S., Christensen, P., 1979. A mechanism of breakdown of limestone nodules in a freeze-thaw environment. Cem. Concr. Res. 9, 741–746. https://doi.org/10.1016/0008-8846(79)90069-3.
Chau, K.T., Shao, J.F., 2006. Subcritical crack growth of edge and center cracks in façade rock panels subject to periodic surface temperature variations. Int. J. Solids Struct. 43, 807–827. https://doi.org/10.1016/J.IJSOLSTR.2005.07.010.
Chen, T.C.C., Yeung, M.R.R., Mori, N., 2004. Effect of water saturation on deterioration of welded tuff due to freeze-thaw action. Cold Reg. Sci. Technol. 38, 127–136.
Cnudde, V., Boone, M.N., 2013. High-resolution X-ray computed tomography in geosciences: a review of the current technology and applications. Earth-Sci. Rev. 123, 1–17. https://doi.org/10.1016/j.earscirev.2013.04.003.
Coletti, C., Cultrone, G., Maritan, L., Mazzoli, C., 2016. Combined multi-analytical approach for study of pore system in bricks: how much porosity is there? Mater. Charact. 121, 82–92. https://doi.org/10.1016/J.MATCHAR.2016.09.024.
Corr, D.J., Monteiro, P.J.M., Bastacky, J., 2002. Microscopic characterization of ice morphology in entrained air voids. ACI Mater. J. 99, 190–195 Doi: 10.14359/11712.
Corr, D.J., Juenger, M.C.G., Monteiro, P.J.M., Bastacky, J., 2004. Investigating entrained air voids and Portland cement hydration with low-temperature scanning electron microscopy. Cem. Concr. Compos. 26, 1007–1012. https://doi.org/10.1016/J.CEMCONCOMP.2004.02.035.
Correns, C.W., Steinborn, W., 1939. Experimente zur Messung Und Erklärung der sogenannten Kristallisationskraft. Zeitschrift für Krist. Mater. 101, 117–133.
Coussy, O., 2004. Poromechanics. John Wiley & Sons, Ltd, Chichester, West Sussex, England.
Coussy, O., 2006. Deformation and stress from in-pore drying-induced crystallization of salt. J. Mech. Phys. Solids 54, 1517–1547. https://doi.org/10.1016/j.jmps.2006.03.002.
Coussy, O., Monteiro, P., 2007. Unsaturated poroelasticity for crystallization in pores. Comput. Geotech. 34, 279–290.
Coussy, O., Monteiro, P.J.M., 2008. Poroelastic model for concrete exposed to freezing temperatures. Cem. Concr. Res. 38, 40–48. https://doi.org/10.1016/J.CEMCONRES.2007.06.006.
Cultrone, G., Sebastián, E., Elert, K., de la Torre, M.J., Cazalla, O., Rodriguez-Navarro, C., 2004. Influence of mineralogy and firing temperature on the porosity of bricks. J. Eur. Ceram. Soc. 24, 547–564. https://doi.org/10.1016/S0955-2219(03)00249-8.
Dagesse, D.F., 2013. Freezing cycle effects on water stability of soil aggregates. Can. J. Soil Sci. 93, 473–483. https://doi.org/10.4141/cjss2012-046.
de Argandoña, V.G.R., Rey, A.R., Celorio, C., del Río, L.M.S., Calleja, L., Llavona, J., 1999. Characterization by computed X-ray tomography of the evolution of the pore structure of a dolomite rock during freeze-thaw cyclic tests. Phys. Chem. Earth, Part A Solid Earth Geod. 24, 633–637. https://doi.org/10.1016/S1464-1895(99)00092-7.
De Boever, W., Derluyn, H., Van Loo, D., Van Hoorebeke, L., Cnudde, V., 2015. Data-fusion of high resolution X-ray CT, SEM and EDS for 3D and pseudo-3D chemical and structural characterization of sandstone. Micron 74, 15–21. https://doi.org/10.1016/J.MICRON.2015.04.003.
De Kock, T., Boone, M.A., De Schryver, T., Van Stappen, J., Derluyn, H., Masschaele, B., Geert, Schutter, D., Cnudde, V., 2015. A Pore-scale study of fracture dynamics in rock using X-ray micro- CT under ambient freeze – thaw cycling. Environ. Sci. Technol. 49, 2867–2874. https://doi.org/10.1021/es505738d.
De Kock, T., Turmel, A., Fronteau, G., Cnudde, V., 2017. Rock fabric heterogeneity and its influence on the petrophysical properties of a building limestone: Lede stone (Belgium) as an example. Eng. Geol. 216, 31–41. https://doi.org/10.1016/J.ENGGEO.2016.11.007.
De Schutter, G., 2012. Damage to concrete structures. In: CRC Press. Taylor and Francis, Group.
De Yoreo, J.J., Vekilov, P.G., 2003. Principles of Crystal Nucleation and growth. Rev. Mineral. Geochem. 54, 57–93.
Debenedetti, P.G., 2003. Supercooled and glassy water. J. Phys. Condens. Matter 15, 1669–1726.
Deprez, M., De Kock, T., De Schutter, G., Cnudde, V., 2017. Dynamic X-ray CT to monitor water distribution within porous building materials: a build-up towards frost-related experiments. In: 3rd International Conference on Tomography of Materials and Structures. Lund, Sweden.
Deprez, M., De Kock, T., De Schutter, G., Cnudde, V., 2020. The role of ink-bottle pores in freeze-thaw damage of oolithic limestone. Construction and Building Materials 246 (118515), 1–12. https://doi.org/10.1016/j.conbuildmat.2020.118515.
Dewanckele, J., Boone, M.A., De Kock, T., De Boever, W., Brabant, L., Boone, M.N., Fronteau, G., Dils, J., Van Hoorebeke, L., Jacobs, P., Cnudde, V., 2013. Holistic approach of pre-existing flaws on the decay of two limestones. Sci. Total Environ. 447, 403–414. https://doi.org/10.1016/J.SCITOTENV.2012.12.094.
Diamond, S., 2000. Mercury porosimetry: an inappropriate method for the measurement of pore size distributions in cement-based materials. Cem. Concr. Res. 30, 1517–1525. https://doi.org/10.1016/S0008-8846(00)00370-7.
Dierick, M., Van Loo, D., Masschaele, B., Van Den Bulcke, J., Van Acker, J., Cnudde, V., Van Hoorebeke, L., 2014. Recent micro-CT scanner developments at UGCT. Nucl. Instruments Methods Phys. Res. Sect. B Beam Interact. with Mater. Atoms 324, 35–40. https://doi.org/10.1016/j.nimb.2013.10.051.
Draebing, D., Krautblatter, M., Hoffmann, T., 2017. Thermo-cryogenic controls of fracture kinematics in permafrost rockwalls. Geophys. Res. Lett. 44, 3535–3544. https://doi.org/10.1002/2016GL072050.
Du, L., Folliard, K.J., 2005. Mechanisms of air entrainment in concrete. Cem. Concr. Res. 35, 1463–1471. https://doi.org/10.1016/j.cemconres.2004.07.026.
Duca, S., Occhiena, C., Mattone, M., Sambuelli, L., Scavia, C., 2014. Feasibility of Ice segregation location by acoustic emission detection: a laboratory test in gneiss. Permafr. Periglac. Process. 25, 208–219. https://doi.org/10.1002/ppp.1814.
Eppes, M.C., Keanini, R., 2017. Mechanical weathering and rock erosion by climate-dependent subcritical cracking. Rev. Geophys. 55, 470–508. https://doi.org/10.1002/2017RG000557.
Eppes, M.C., Magi, B., Hallet, B., Delmelle, E., Mackenzie-Helnwein, P., Warren, K., Swami, S., 2016. Deciphering the role of solar-induced thermal stresses in rock weathering. Bull. Geol. Soc. Am. 128, 1315–1338. https://doi.org/10.1130/B31422.1.
Eriksson, D., Gasch, T., Malm, R., Ansell, A., 2018. Freezing of partially saturated air-entrained concrete: a multiphase description of the hygro-thermo-mechanical behaviour. Int. J. Solids Struct. 152–153, 294–304. https://doi.org/10.1016/J.IJSOLSTR.2018.07.004.
Espinosa-Marzal, R.M., Hamilton, A., McNall, M., Whitaker, K., Scherer, G.W., 2011. The chemomechanics of crystallization during rewetting of limestone impregnated with sodium sulfate. J. Mater. Res. 26, 1472–1481. https://doi.org/10.1557/jmr.2011.137.
Everett, D.H., 1961. The thermodynamics of frost damage to porous solids. Trans. Faraday Soc. 57, 1541. https://doi.org/10.1039/tf9615701541.
Fabbri, A., Fen-Chong, T., Coussy, O., 2006. Dielectric capacity, liquid water content, and pore structure of thawing–freezing materials. Cold Reg. Sci. Technol. 44, 52–66. https://doi.org/10.1016/j.coldregions.2005.07.001.
Fabbri, A., Fen-Chong, T., Azouni, A., Thimus, J.-F., 2009. Investigation of water to Ice phase change in porous media by ultrasonic and dielectric measurements. J. Cold Reg. Eng. 23, 69–90. https://doi.org/10.1061/(ASCE)0887-381X(2009)23:2(69).
Fagerlund, G., 1975. The signifcance of critical degrees of saturation at freezing of porous and brittle materials. In: Conf. on Durability of Concrete, ACI STP. New Jersey and Ottawa, Ontario, pp. 13–66. https://doi.org/10.14359/17604.
Fagerlund, G., 1977. The international cooperative test of the critical degree of saturation method of assessing the freeze/thaw resistance of concrete. Mater. Constr. 10, 231–253. https://doi.org/10.1007/BF02478694.
Fagerlund, G., 2004. A Service Life Model for Internal Frost Damage in Concrete.
Feng, X., Nielsen, L.L., Simpson, M.J., 2007. Responses of soil organic matter and microorganisms to freeze–thaw cycles. Soil Biol. Biochem. 39, 2027–2037. https://doi.org/10.1016/j.soilbio.2007.03.003.
Feng, C., Roels, S., Janssen, H., 2019. Towards a more representative assessment of frost damage to porous building materials. Build. Environ. 164, 106343. https://doi.org/10.1016/j.buildenv.2019.106343.
Flatt, R.J., Steiger, M., Scherer, G.W., 2007. A commented translation of the paper by C.W. Correns and W. Steinborn on crystallization pressure. Environ. Geol. 52, 187–203. https://doi.org/10.1007/s00254-006-0509-5.
Gilpin, R.R., 1979. A model for the prediction of ice lensing and frost heave in soils. Water Resour. Res. 16, 918–930. https://doi.org/10.1029/WR016i005p00918.
Gilpin, R.R., 1980. A Model for the Prediction of Ice Lensing and Frost Heave in Soils. Water Resour. Res. 16, 918–930.
Girard, L., Gruber, S., Weber, S., Beutel, J., 2013a. Environmental controls of frost cracking revealed through in situ acoustic emission measurements in steep bedrock. Geophys. Res. Lett. 40, 1748–1753. https://doi.org/10.1002/grl.50384.
Girard, L., Gruber, S., Weber, S., Beutel, J., 2013b. Environmental controls of frost cracking revealed through in situ acoustic emission measurements in steep bedrock. Geophys. Res. Lett. doi. https://doi.org/10.1002/grl.50384.
Griggs, D.T., 1936. The factor of Fatigue in Rock Exfoliation. J. Geol. 44, 783–796. https://doi.org/10.1086/624483.
Groenevelt, P.H., Grant, C.D., 2013. Heave and heaving pressure in freezing soils: a unifying theory. Vadose Zo. J. https://doi.org/10.2136/vzj2012.0051. 12, 0.
Grossi, C.M., Brimblecombe, P., Harris, I., 2007. Predicting long term freeze–thaw risks on Europe built heritage and archaeological sites in a changing climate. Sci. Total Environ. 377, 273–281. https://doi.org/10.1016/J.SCITOTENV.2007.02.014.
Gruber, S., Hoelzle, M., Haeberli, W., 2004. Rock-wall temperatures in the Alps: modelling their topographic distribution and regional differences. Permafr. Periglac. Process. 15, 299–307. https://doi.org/10.1002/ppp.501.
Guilbert, D., Caluwaerts, S., Calle, K., Van Den Bossche, N., Cnudde, V., De Kock, T., 2019. Impact of the urban heat island on freeze-thaw risk of natural stone in the built

environment, a case study in Ghent. Belgium. Sci. Total Environ. 677, 9–18. https://doi.org/10.1016/J.SCITOTENV.2019.04.344.
Guo, E., Kazantsev, D., Mo, J., Bent, J., Van Dalen, G., Schuetz, P., Rockett, P., StJohn, D., Lee, P.D., 2018. Revealing the microstructural stability of a three-phase soft solid (ice cream) by 4D synchrotron X-ray tomography. J. Food Eng. 237, 204–214. https://doi.org/10.1016/j.jfoodeng.2018.05.027.
Hain, M., Wriggers, P., 2008. Computational homogenization of micro-structural damage due to frost in hardened cement paste. Finite Elem. Anal. Des. 44, 233–244. https://doi.org/10.1016/J.FINEL.2007.11.020.
Hales, T.C., Roering, J.J., 2007. Climatic controls on frost cracking and implications for the evolution of bedrock landscapes. J. Geophys. Res. Earth Surf. 112, F02033. https://doi.org/10.1029/2006JF000616.
Hall, K., 1986. Rock moisture content in the field and the laboratory and its relationship to mechanical weathering studies. Earth Surf. Process. Landf. 11, 131–142. https://doi.org/10.1002/esp.3290110204.
Hall, K., 1988. A Laboratory simulation of rock breakdown due to freeze-thaw in a maritime antarctic environment. Earth Surf. Process. Landf. 13, 369–382.
Hall, K., 1997. Rock Temperatures and Implications for Cold Region Weathering. I: New Data from Viking Valley, Alexander Island. Antarctica. Permafr. Periglac. Process. 8, 69–90. https://doi.org/10.1002/(SICI)1099-1530(199701)8. 1 < 69::AID-PPP236 > 3.0.CO;2-Q.
Hall, K., 1998. Rock temperatures and implications for cold region weathering. II: New data from Rothera, Adelaide Island. Antarctica. Permafr. Periglac. Process. 9, 47–55. https://doi.org/10.1002/(SICI)1099-1530(199801/03)9:1 < 47::AID-PPP273 > 3.0.CO;2-N.
Hall, K., 1999. The role of thermal stress fatigue in the breakdown of rock in cold regions. Geomorphology 31, 47–63. https://doi.org/10.1016/S0169-555X(99)00072-0.
Hall, K., 2004. Evidence for freeze–thaw events and their implications for rock weathering in northern Canada. Earth Surf. Process. Landf. 29, 43–57. https://doi.org/10.1002/esp.1012.
Hall, K., 2007. Evidence for freeze–thaw events and their implications for rock weathering in northern Canada: II. The temperature at which water freezes in rock. Earth Surf. Process. Landf. 32, 249–259. https://doi.org/10.1002/esp.1389.
Hall, K., André, M.-F., 2001. New insights into rock weathering from high-frequency rock temperature data: an Antarctic study of weathering by thermal stress. Geomorphology 41, 23–35. https://doi.org/10.1016/S0169-555X(01)00101-5.
Hall, C., Hoff, W.D., 2002. Water Transport in Brick, Stone and Concrete, 1st ed. CRC Press, London. https://doi.org/10.4324/9780203301708.
Hall, K., Thorn, C., 2011. The historical legacy of spatial scales in freeze–thaw weathering: Misrepresentation and resulting misdirection. Geomorphology 130, 83–90. https://doi.org/10.1016/j.geomorph.2010.10.003.
Hallet, B., Walder, J.S., Stubbs, C.W., 1991. Weathering by segregation ice growth in microcracks at sustained subzero temperatures: Verification from an experimental study using acoustic emissions. Permafr. Periglac. Process. 2, 283–300. https://doi.org/10.1002/ppp.3430020404.
Hasler, A., Gruber, S., Haeberli, W., 2011. Temperature variability and offset in steep alpine rock and ice faces. Cryosph. 5, 977–988. https://doi.org/10.5194/tc-5-977-2011.
Hasler, A., Gruber, S., Beutel, J., 2012. Kinematics of steep bedrock permafrost. J. Geophys. Res. Earth Surf. 117https://doi.org/10.1029/2011JF001981. n/a-n/a.
Hassine, M.A., Beck, K., Brunetaud, X., Al-Mukhtar, M., 2018. Use of electrical resistance measurement to assess the water saturation profile in porous limestones during capillary imbibition. Constr. Build. Mater. 165, 206–217. https://doi.org/10.1016/J.CONBUILDMAT.2017.12.238.
Hauck, C., 2002. Frozen ground monitoring using DC resistivity tomography. Geophys. Res. Lett. 29, 2016. https://doi.org/10.1029/2002GL014995.
Henry, H.A.L., 2007. Soil freeze-thaw cycle experiments: Trends, methodological weaknesses and suggested improvements. Soil Biol. Biochem. doi. https://doi.org/10.1016/j.soilbio.2006.11.017.
Hillig, W.B., Turnbull, D., 1956. Theory of Crystal Growth in Undercooled Pure Liquids. J. Chem. Phys. 24, 914. https://doi.org/10.1063/1.1742646.
Hirschwald, J., 1908. Die Prüfung der natürlichen Bausteine auf ihre Wetterfeständigkeit. W. Ernst & Sohn.
Ingham, J.P., 2005. Predicting the frost resistance of building stone. Q. J. Eng. Geol. Hydrogeol. 38, 387–399. https://doi.org/10.1144/1470-9236/04-068.
Isaksen, K., Ødegård, R.S., Etzelmüller, B., Hilbich, C., Hauck, C., Farbrot, H., Eiken, T., Hygen, H.O., Hipp, T.F., 2011. Degrading Mountain Permafrost in Southern Norway: Spatial and Temporal Variability of mean Ground Temperatures, 1999-2009. Permafr. Periglac. Process. 22, 361–377. https://doi.org/10.1002/ppp.728.
Ishikawa, M., Kurashige, Y., Hirakawa, K., 2004. Analysis of crack movements observed in an alpine bedrock cliff. Earth Surf. Process. Landf. 29, 883–891. https://doi.org/10.1002/esp.1076.
Israelachvili, J.N., 2011. Intermolecular and Surface Forces, 3rd ed. Academic Press.
Jacobsen, S., Marchand, J., Hornain, H., 1995. Sem observations of the microstructure of frost deteriorated and self-healed concretes. Cem. Concr. Res. 25, 1781–1790. https://doi.org/10.1016/0008-8846(95)00174-3.
Jehng, J.-Y., Sprague, D.T., Halperin, W.P., 1996. Pore structure of hydrating cement paste by magnetic resonance relaxation analysis and freezing. Magn. Reson. Imaging 148, 785–791.
Johannesson, B., 2010. Dimensional and ice content changes of hardened concrete at different freezing and thawing temperatures. Cem. Concr. Compos. 32, 73–83. https://doi.org/10.1016/j.cemconcomp.2009.09.001.
Kalikmanov, V.I., 2013. Nucleation Theory. Springer.
Katz, A.J., Thompson, A.H., 1986. Quantitative prediction of permeability in porous rock. Phys. Rev. B 34, 8179–8181.
Kaufmann, J.P., 2004. Experimental identification of ice formation in small concrete pores. Cem. Concr. Res. 34, 1421–1427. https://doi.org/10.1016/j.cemconres.2004.01.022.
Kemeny, J.M., 1991. A model for non-linear rock deformation under compression due to sub-critical crack growth. Int. J. Rock Mech. Min. Sci. Geomech. Abstr. 28, 459–467. https://doi.org/10.1016/0148-9062(91)91121-7.
Kneisel, C., Hauck, C., Fortier, R., Moorman, B., 2008. Advances in geophysical methods for permafrost investigations. Permafr. Periglac. Process. 19, 157–178. https://doi.org/10.1002/ppp.616.
Koniorczyk, M., Konca, P., 2017. Kinetics of water freezing in mesopores determined by differential scanning calorimetry. Int. J. Therm. Sci. 122, 124–132. https://doi.org/10.1016/j.ijthermalsci.2017.08.015.
Koniorczyk, M., Gawin, D., Schrefler, B.A., 2015. Modeling evolution of frost damage in fully saturated porous materials exposed to variable hygro-thermal conditions. Comput. Methods Appl. Mech. Eng. 297, 38–61. https://doi.org/10.1016/J.CMA.2015.08.015.
Koponen, H.T., Martikainen, P.J., 2004. Soil water content and freezing temperature affect freeze–thaw related N $_2$ O production in organic soil. Nutr. Cycl. Agroecosyst. 69, 213–219. https://doi.org/10.1023/B:FRES.0000035172.37839.24.
Kordatos, E.Z., Exarchos, D.A., Stavrakos, C., Moropoulou, A., Matikas, T.E., 2013. Infrared thermographic inspection of murals and characterization of degradation in historic monuments. Constr. Build. Mater. 48, 1261–1265. https://doi.org/10.1016/J.CONBUILDMAT.2012.06.062.
Krautblatter, M., Dikau, R., 2007. Towards a uniform concept for the comparison and extrapolation of Rockwall retreat and rockfall supply. Geogr. Ann. Ser. A Phys. Geogr. 89, 21–40. https://doi.org/10.1111/j.1468-0459.2007.00305.x.
Krautblatter, M., Hauck, C., 2007. Electrical resistivity tomography monitoring of permafrost in solid rock walls. J. Geophys. Res. 112, F02S20. https://doi.org/10.1029/2006JF000546.
Krautblatter, M., Moser, M., 2009. A nonlinear model coupling rockfall and rainfall intensity based on a four year measurement in a high Alpine rock wall (Reintal, German Alps). Nat. Hazards Earth Syst. Sci. 9, 1425–1432. https://doi.org/10.5194/nhess-9-1425-2009.
Krautblatter, M., Moser, M., Dikau, R., 2006. Nonlinear response of small-scale rockfall activity to rainfall intensity: the importance of gross secondary rockfall events. In: Geophysical Research Abstracts, pp. 10895.
Kruschwitz, J., Bluhm, J., 2005. Modeling of ice formation in porous solids with regard to the description of frost damage. Comput. Mater. Sci. 32, 407–417. https://doi.org/10.1016/J.COMMATSCI.2004.09.025.
Künzel, H.M., 1995. Simultaneous Heat and Moisture Transport in Building Components: One-and two-dimensional calculation using simple parameters, Fraunhofer IRB Verlag Suttgart.
Künzel, H.M., 1998. Effect of interior and exterior insulation on the hygrothermal behaviour of exposed walls. Mater. Struct. 31, 99–103. https://doi.org/10.1007/BF02486471.
Kuras, O., Meldrum, P.I., Haslam, E.P., Wilkinson, P.B., Krautblatter, M., Murton, J.B., Ogilvy, R.D., 2011. Time-lapse capacitive resistivity imaging - A novel methodology for the monitoring of permafrost processes in bedrock, in: Near Surface 2011 - 17th European Meeting of Environmental and Engineering Geophysics. Environ. Eng. Geophys. Soc. 13–16. https://doi.org/10.4133/1.4721680.
Kurylyk, B.L., Watanabe, K., 2013. The mathematical representation of freezing and thawing processes in variably-saturated, non-deformable soils. Adv. Water Resour. 60, 160–177. https://doi.org/10.1016/j.advwatres.2013.07.016.
Landry, M.R., 2005. Thermoporometry by differential scanning calorimetry: experimental considerations and applications. Thermochim. Acta 433, 27–50. https://doi.org/10.1016/J.TCA.2005.02.015.
Lavalle, J., 1853. Recherches sur la formation lente de cristaux à températures ordinaire. C. R. Acad. Sci. 36, 493–495.
Li, W., Pour-Ghaz, M., Asce, M., Castro, J., Weiss, J., 2012. Water absorption and critical degree of saturation relating to freeze-thaw damage in concrete pavement joints background on the problem of joint deterioration in concrete pavements. J. Mater. Civ. Eng. 24, 299–307. https://doi.org/10.1061/(ASCE)MT.1943-5533.0000383.
Li, J., Kaunda, R.B., Zhou, K., 2018. Experimental investigations on the effects of ambient freeze-thaw cycling on dynamic properties and rock pore structure deterioration of sandstone. Cold Reg. Sci. Technol. 154, 133–141. https://doi.org/10.1016/J.COLDREGIONS.2018.06.015.
Lisø, K.R., Kvande, T., Hygen, H.O., Thue, J.V., Harstveit, K., 2007. A frost decay exposure index for porous, mineral building materials. Build. Environ. 42, 3547–3555. https://doi.org/10.1016/J.BUILDENV.2006.10.022.
Litvan, G.G., 1972. Phase transitions'of adsorbates III. heat effects and dimensional changes in nonequilibrium temperature cycles. J. Colloid Interface Sci. 38, 75–83.
Litvan, G.G., 1978. Adsorption systems at temperatures below the freezing point of the adsorptive. Adv. Colloid Interf. Sci. 9, 253–302. https://doi.org/10.1016/0001-8686(78)85001-5.
Liu, L., Ye, G., Schlangen, E., Chen, H., Qian, Z., Sun, W., van Breugel, K., 2011. Modeling of the internal damage of saturated cement paste due to ice crystallization pressure during freezing. Cem. Concr. Compos. 33, 562–571. https://doi.org/10.1016/J.CEMCONCOMP.2011.03.001.
Liu, L., Shen, D., Chen, H., Sun, W., Qian, Z., Zhao, H., Jiang, J., 2014. Analysis of damage development in cement paste due to ice nucleation at different temperatures. Cem. Concr. Compos. 53, 1–9.
Luckman, B.H., 1976. Rockfalls and rockfall inventory data : some observations from surprise valley. Jasper National Park. Earth Surf. Process. 1, 287–298.
Ludwig, W., King, A., Reischig, P., Herbig, M., Lauridsen, E.M., Schmidt, S., Proudhon, H., Forest, S., Cloetens, P., du Roscoat, S.R., Buffière, J.Y., Marrow, T.J., Poulsen, H.F., 2009. New opportunities for 3D materials science of polycrystalline materials at the micrometre lengthscale by combined use of X-ray diffraction and X-ray imaging.

Mater. Sci. Eng. A 524, 69–76. https://doi.org/10.1016/J.MSEA.2009.04.009.
Luetschg, M., Stoeckli, V., Lehning, M., Haeberli, W., Ammann, W., 2004. Temperatures in two boreholes at Flüela Pass, eastern Swiss Alps: the effect of snow redistribution on permafrost distribution patterns in high mountain areas. Permafr. Periglac. Process. 15, 283–297. https://doi.org/10.1002/ppp.500.
Maage, M., 1984. Frost resistance and pore size distribution in bricks. Mater. Constr. 17, 345–350. https://doi.org/10.1007/BF02478706.
Martinez-Martinez, J., Benavente, D., Gomez-Heras, M., Marco-Castano, L., Garcia-Del-Cura, M.A., 2013. Non-linear decay of building stones during freeze-thaw weathering processes. Constr. Build. Mater. 38, 443–454. https://doi.org/10.1016/j.conbuildmat.2012.07.059.
Martins, L., Vasconcelos, G., Lourenço, P.B., Palha, C., 2016. Influence of the Freeze-Thaw Cycles on the Physical and Mechanical Properties of Granites. J. Mater. Civ. Eng. 28, 04015201. https://doi.org/10.1061/(ASCE)MT.1943-5533.0001488.
Matsuoka, N., 1990a. Mechanism of rock breakdown by frost action: an experimental approach. Cold Reg. Sci. Technol. 17, 253–270. https://doi.org/10.1016/S0165-232X(05)80005-9.
Matsuoka, N., 1990b. The rate of bedrock weathering by frost action: Field measurements and a predictive model. Earth Surf. Process. Landf. 15, 73–90. https://doi.org/10.1002/esp.3290150108.
Matsuoka, N., 1994. Diurnal freeze–thaw depth in rockwalls: Field measurements and theoretical considerations. Earth Surf. Process. Landf. 19, 423–435. https://doi.org/10.1002/esp.3290190504.
Matsuoka, N., 2001a. Direct observation of frost wedging in alpine bedrock. Earth Surf. Process. Landf. 26, 601–614. https://doi.org/10.1002/esp.208.
Matsuoka, N., 2001b. Microgelivation versus macrogelivation: towards bridging the gap between laboratory and field frost weathering. Permafr. Periglac. Process. 12, 299–313. https://doi.org/10.1002/ppp.393.
Matsuoka, N., 2008. Frost weathering and Rockwall erosion in the southeastern Swiss Alps: long-term (1994-2006) observations. Geomorphology. https://doi.org/10.1016/j.geomorph.2007.11.013.
Matsuoka, N., 2019. A multi-method monitoring of timing, magnitude and origin of rockfall activity in the Japanese Alps. Geomorphology 336, 65–76. https://doi.org/10.1016/j.geomorph.2019.03.023.
Matsuoka, N., Murton, J., 2008. Frost weathering: recent advances and future directions. Permafr. Periglac. Process. 19, 195–210. https://doi.org/10.1002/ppp.620.
Matsuoka, N., Sakai, H., 1999. Rockfall activity from an alpine cliff during thawing periods. Geomorphology 28, 309–328. https://doi.org/10.1016/S0169-555X(98)00116-0.
Matsuoka, N., Hirakawa, K., Watanabe, T., Moriwaki, K., 1997. Monitoring of periglacial slope processes in the Swiss Alps: the first two years of frost shattering, heave and creep. Permafr. Periglac. Process. 8, 155–177. https://doi.org/10.1002/(SICI)1099-1530(199732)8:2<155::AID-PPP248>3.0.CO;2-N.
Matthews, J.A., Dawson, A.G., Shakesby, R.A., 1986. Lake shoreline development, frost weathering and rock platform erosion in an alpine periglacial environment, Jotunheimen, southern Norway. Boreas 15, 33–50. https://doi.org/10.1111/j.1502-3885.1986.tb00741.x.
McAllister, D., McCabe, S., Smith, B.J.J., Srinivasan, S., Warke, P.A.A., 2013. Low temperature conditions in building sandstone: the role of extreme events in temperate environments. Eur. J. Environ. Civ. Eng. 17, 99–112. https://doi.org/10.1080/19648189.2012.751225.
McGreevy, J.P., Whalley, W.B., 1985. Rock moisture content and frost weathering under natural and experimental conditions: a comparative discussion. Arct. Alp. Res. 17, 337–346. https://doi.org/10.2307/1551022.
Merriam, R., Rieke, H.H., Kim, Y.C., 1970. Tensile strength related to mineralogy and texture of some granitic rocks. Eng. Geol. 4, 155–160. https://doi.org/10.1016/0013-7952(70)90010-4.
Meyers, S.L., 1951. Thermal expansion characteristics of hardened cement paste and of concrete. Highw. Res. Board Proc. 30, 193–203.
Miller, R.D., 1972. Freezing and Heaving of Saturated and Unsaturated Soils. Highw. Res. Rec.
Mol, L., Viles, H.A., 2010. Geoelectric investigations into sandstone moisture regimes: Implications for rock weathering and the deterioration of San Rock Art in the Golden Gate Reserve, South Africa. Geomorphology 118, 280–287. https://doi.org/10.1016/J.GEOMORPH.2010.01.008.
Moropoulou, A., Labropoulos, K.C., Delegou, E.T., Karoglou, M., Bakolas, A., 2013. Non-destructive techniques as a tool for the protection of built cultural heritage. Constr. Build. Mater. 48, 1222–1239. https://doi.org/10.1016/J.CONBUILDMAT.2013.03.044.
Mosquera, M.J., Rivas, T., Prieto, B., Silva, B., 2000. Capillary rise in Granitic Rocks: Interpretation of Kinetics on the Basis of Pore Structure. J. Colloid Interface Sci. 222, 41–45. https://doi.org/10.1006/JCIS.1999.6612.
Müller, J., Gärtner-Roer, I., Kenner, R., Thee, P., Morche, D., 2014. Sediment storage and transfer on a periglacial mountain slope (Corvatsch, Switzerland). Geomorphology 218, 35–44. https://doi.org/10.1016/j.geomorph.2013.12.002.
Murton, J.B., 1996. Near-surface brecciation of chalk, isle of thanet, south-east England: a comparison with ice-rich brecciated bedrocks in Canada and Spitsbergen. Permafr. Periglac. Process. 7, 153–164. https://doi.org/10.1002/(sici)1099-1530(199604)7:2<153::aid-ppp215>3.0.co;2–7.
Murton, J.B., Coutard, J.P., Lautridou, J.P., Ozouf, J.C., Robinson, D.A., Williams, R.B.G., Guillemet, G., Simmons, P., 2000. Experimental Design for a Pilot Study on Bedrock Weathering near the Permafrost Table, in: Earth Surface Processes and Landforms. John Wiley & Sons, Ltd, pp. 1281–1294. https://doi.org/10.1002/1096-9837(200011)25:12<1281::AID-ESP137>3.0.CO;2-U.
Murton, J.B., Peterson, R., Ozouf, J.-C., 2006. Bedrock fracture by ice segregation in cold regions. Science 314, 1127–1129. https://doi.org/10.1126/science.1132127.
Mutou, Y., Watanabe, K., Ishizaki, T., Mizoguchi, M., 1998. Microscopic Observation of Ice Lensing and Frost Heaves in Glass Beads. In: Lewkowicz, A.G., Allard, M. (Eds.), Proceedings of the 7th International Conference on Permafrost. Yellowknife, NWT, Canada, pp. 783–787.
Nicholson, D.T., Nicholson, F.H., 2000. Physical deterioration of sedimentary rocks subjected to experimental freeze-thaw weathering. Earth Surf. Process. Landf. 25, 1295–1307. https://doi.org/10.1002/1096-9837(200011)25:12<1295::AID-ESP138>3.0.CO;2-E.
Nicolai, A., Grunewald, J., Zhang, J.J., 2007. Recent improvements in HAM simulation tools: Delphin 5 / CHAMPS-BES. In: Conference Proceedings of 12th Symposium of Building Physics, pp. 866–876.
Orr, S.A., Viles, H.A., Leslie, A.B., Stelfox, D., 2016. Comparability of non-destructive moisture measurement techniques on masonry during simulated wetting. In: Hughes, J.J., Howind, T. (Eds.), Proceedings of the 13th International Congress on the Deterioration and Conservation of Stone. University of the West of Scotland, Paisley, pp. 431–438.
Orr, S.A., Fusade, L., Young, M., Stelfox, D., Leslie, A., Curran, J., Viles, H., 2019a. Moisture monitoring of stone masonry: a comparison of microwave and radar on a granite wall and a sandstone tower. J. Cult. Herit. https://doi.org/10.1016/J.CULHER.2019.07.011.
Orr, S.A., Young, M., Stelfox, D., Leslie, A., Curran, J., Viles, H., 2019b. An 'isolated diffusion' gravimetric calibration procedure for radar and microwave moisture measurement in porous building stone. J. Appl. Geophys. 163, 1–12. https://doi.org/10.1016/J.JAPPGEO.2019.02.003.
Outcalt, S.I., Nelson, F.E., Hinkel, K.M., 1990. The zero-curtain effect: Heat and mass transfer across an isothermal region in freezing soil. Water Resour. Res. 26, 1509–1516. https://doi.org/10.1029/WR026i007p01509.
Oztas, T., Fayetorbay, F., 2003. Effect of freezing and thawing processes on soil aggregate stability. Catena 52, 1–8. https://doi.org/10.1016/S0341-8162(02)00177-7.
Peppin, S.S.L., Style, R.W., 2013. The physics of frost heave and ice-lens growth. Vadose Zo. J. 12. https://doi.org/10.2136/vzj2012.0049.
Perron, S., Beaudoin, J.J., 2002. Freezing of water in portland cement paste – an ac impedance spectroscopy study. Cem. Concr. Compos. 24, 467–475.
Phillips, M., Haberkorn, A., Draebing, D., Krautblatter, M., Rhyner, H., Kenner, R., 2016. Seasonally intermittent water flow through deep fractures in an Alpine Rock Ridge: Gemsstock. Central Swiss Alps. Cold Reg. Sci. Technol. 125, 117–127. https://doi.org/10.1016/J.COLDREGIONS.2016.02.010.
Powers, T.C., 1945. A Working hypothesis for further studies of frost resistance of concrete. In: Journal Proceedings- American Concrete Institute, pp. 245 Doi: 10.14359/8684.
Powers, T.C., 1949. The air requirement of frost resistant concrete. Highw. Res. Board Proc. 29, 184–211.
Powers, T.C., 1975. Freezing effects in concrete. Spec. Publ. 47, 1–12.
Powers, T.C., Brownyard, T.L., 1946. Studies of the physical properties of hardened portland cement paste. ACI J. Proc. 43, 101–132 Doi: 10.14359/8745.
Powers, T.C., Helmuth, R.A., 1953. Theory of volume changes in hardened portland-cement paste during freezing. Highw. Res. Board Proc. 32.
Prado, P.J., Balcom, B.J., Beyea, S.D., Bremner, T.W., Armstrong, R.L., Grattan-Bellew, P.E., 1998. Concrete freeze/thaw as studied by magnetic resonance imaging. Cem. Concr. Res. 28, 261–270.
Prick, A., 1995. Dilatometrical behaviour of porous calcareous rock samples subjected to freeze-thaw cycles. CATENA 25, 7–20. https://doi.org/10.1016/0341-8162(94)00038-G.
Prick, A., 1997. Critical Degree of Saturation as a Threshold Moisture Level in Frost Weathering of Limestones. Permafr. Periglac. Process. 8, 91–99. https://doi.org/10.1002/(SICI)1099-1530(199701)8:1<91::AID-PPP238>3.0.CO;2-4.
Promentilla, M.A.B., Sugiyama, T., 2010. X-Ray Microtomography of Mortars Exposed to Freezing-Thawing Action. J. Adv. Concr. Technol. 8, 97–111. https://doi.org/10.3151/jact.8.97.
Rempel W., A., 2010. Frost heave. Journal of Glaciology 56 (200), 1122–1128. https://doi.org/10.3189/002214311796406149.
Rempel, A.W., 2012. Hydromechanical processes in freezing soils. Vadose Zo. J. https://doi.org/10.2136/vzj2012.0045.
Rempel, A.W., Wettlaufer, J.S., Worster, M.G., 2004. Premelting dynamics in a continuum model of frost heave. J. Fluid Mech. 498, 227–244. https://doi.org/10.1017/S0022112003006761.
Revol, V., Jerjen, I., Kottler, C., Schtz, P., Kaufmann, R., Lthi, T., Sennhauser, U., Straumann, U., Urban, C., 2011. Sub-pixel porosity revealed by x-ray scatter dark field imaging. J. Appl. Phys. 110, 044912. https://doi.org/10.1063/1.3624592.
Rode, M., Schnepfleitner, H., Sass, O., 2016. Simulation of moisture content in alpine rockwalls during freeze-thaw events. Earth Surf. Process. Landf. 41, 1937–1950. https://doi.org/10.1002/esp.3961.
Ruedrich, J., Siegesmund, S., 2007. Salt and ice crystallisation in porous sandstones. Environ. Geol. 52, 225–249. https://doi.org/10.1007/s00254-006-0585-6.
Ruedrich, J., Kirchner, D., Siegesmund, S., 2011. Physical weathering of building stones induced by freeze–thaw action: a laboratory long-term study. Environ. Earth Sci. 63, 1573–1586. https://doi.org/10.1007/s12665-010-0826-6.
Samouëlian, A., Cousin, I., Tabbagh, A., Bruand, A., Richard, G., 2005. Electrical resistivity survey in soil science: a review. Soil Tillage Res. 83, 173–193. https://doi.org/10.1016/J.STILL.2004.10.004.
Sandrolini, F., Franzoni, E., 2006. An operative protocol for reliable measurements of moisture in porous materials of ancient buildings. Build. Environ. 41, 1372–1380. https://doi.org/10.1016/J.BUILDENV.2005.05.023.
Sass, O., 2004. Rock moisture fluctuations during freeze-thaw cycles: preliminary results from electrical resistivity measurements. Polar Geogr. 28, 13–31. https://doi.org/10.1080/789610157.

Sass, O., 2005a. Rock moisture measurements: techniques, results, and implications for weathering. Earth Surf. Process. Landf. 30, 359–374. https://doi.org/10.1002/esp.1214.
Sass, O., 2005b. Temporal variability of rockfall in the Bavarian Alps, Germany. Arctic. Antarct. Alp. Res. 37, 564–573. https://doi.org/10.1657/1523-0430(2005)037[0564:TVORIT]2.0.CO;2.
Sass, O., Krautblatter, M., 2007. Debris flow-dominated and rockfall-dominated talus slopes: Genetic models derived from GPR measurements. Geomorphology 86, 176–192. https://doi.org/10.1016/j.geomorph.2006.08.012.
Sass, O., Oberlechner, M., 2012. Is climate change causing increased rockfall frequency in Austria? Nat. Hazards Earth Syst. Sci. 12. https://doi.org/10.5194/nhess-12-3209-2012.
Sass, O., Viles, H.A., 2006. How wet are these walls? Testing a novel technique for measuring moisture in ruined walls. J. Cult. Herit. 7, 257–263. https://doi.org/10.1016/J.CULHER.2006.08.001.
Sass, O., Viles, H.A., 2010. Wetting and drying of masonry walls: 2D-resistivity monitoring of driving rain experiments on historic stonework in Oxford. UK. J. Appl. Geophys. 70, 72–83. https://doi.org/10.1016/J.JAPPGEO.2009.11.006.
Scherer, G.W., 1993. Freezing gels. J. Non-Cryst. Solids 155, 1–25. https://doi.org/10.1016/0022-3093(93)90467-C.
Scherer, G.W., 1999. Crystallization in pores. Cem. Concr. Res. 29, 1347–1358. https://doi.org/10.1016/S0008-8846(99)00002-2.
Scherer, G.W., 2004. Stress from crystallization of salt. Cem. Concr. Res. 34, 1613–1624. https://doi.org/10.1016/j.cemconres.2003.12.034.
Scherer, G.W., 2006. Internal Stress and Cracking in Stone and Masonry, in: Measuring. Monitoring and Modeling Concrete Properties. Springer Netherlands, Dordrecht, pp. 633–641. https://doi.org/10.1007/978-1-4020-5104-3_77.
Scherer, G.W., Valenza, J.J., 2005. Mechanisms of frost damage. Mater. Sci. Concr. VII 209–246.
Schneider, S., Hoelzle, M., Hauck, C., 2012. Influence of surface and subsurface heterogeneity on observed borehole temperatures at a mountain permafrost site in the Upper Engadine, Swiss Alps. Cryosphere 6, 517–531. https://doi.org/10.5194/tc-6-517-2012.
Schubert, F., 2004. Basic principles of acoustic emission tomography. In: DGZfP-Proceedings BB 90-CD (EWGAE), pp. 575–585.
Schwartz, B.F., Schreiber, M.E., Yan, T., 2008. Quantifying field-scale soil moisture using electrical resistivity imaging. J. Hydrol. 362, 234–246. https://doi.org/10.1016/J.JHYDROL.2008.08.027.
Sedlbauer, K., Künzel, H.M., 2000. Frost damage of Masonry Walls – a hygrothermal Analysis by Computer Simulations. J. Therm. Envel. Build. Sci. 23, 277–281.
Sellberg, J.A., Huang, C., McQueen, T.A., Loh, N.D., Laksmono, H., Schlesinger, D., Sierra, R.G., Nordlund, D., Hampton, C.Y., Starodub, D., DePonte, D.P., Beye, M., Chen, C., Martin, A.V., Barty, A., Wikfeldt, K.T., Weiss, T.M., Caronna, C., Feldkamp, J., Skinner, L.B., Seibert, M.M., Messerschmidt, M., Williams, G.J., Boutet, S., Pettersson, L.G.M., Bogan, M.J., Nilsson, A., 2014. Ultrafast X-ray probing of water structure below the homogeneous ice nucleation temperature. Nature 510, 381–384. https://doi.org/10.1038/nature13266.
Shea, W.T., Kronenberg, A.K., 1993. Strength and anisotropy of foliated rocks with varied mica contents. J. Struct. Geol. 15, 1097–1121. https://doi.org/10.1016/0191-8141(93)90158-7.
Shields, Y., Garboczi, E., Weiss, J., Farnam, Y., 2018. Freeze-thaw crack determination in cementitious materials using 3D X-ray computed tomography and acoustic emission. Cem. Concr. Compos. doi. https://doi.org/10.1016/j.cemconcomp.2018.03.004.
Shimada, H., Sakai, K., Litvan, G.G., 1991. Acoustic emissions of mortar subjected to freezing and thawing. Spec. Publ. 126, 263–278 Doi: 10.14359/2159.
Snethlage, R., Wendler, E., 1997. Moisture cycles and sandstone degradation. Environ. Sci. Res. Rep. 20, 7–24.
Snoeck, D., 2016. Self-Healing and Microstructure of Cementitious Materials with Microfibres and Superabsorbent Polymers. Ghent University.
Steelman, C.M., Endres, A.L., van der Kruk, J., 2010. Field observations of shallow freeze and thaw processes using high-frequency ground-penetrating radar. Hydrol. Process. 24https://doi.org/10.1002/hyp.7688. n/a-n/a.
Steiger, M., 2005a. Crystal growth in porous materials—I: the crystallization pressure of large crystals. J. Cryst. Growth 282, 455–469. https://doi.org/10.1016/j.jcrysgro.2005.05.007.
Steiger, M., 2005b. Crystal growth in porous materials—II: Influence of crystal size on the crystallization pressure. J. Cryst. Growth 282, 470–481. https://doi.org/10.1016/j.jcrysgro.2005.05.008.
Steiger, M., Charola, A.E., Sterflinger, K., 2014. Stone in Architecture. In: Siegesmund, S., Snethlage, R. (Eds.), Stone in Architecture: Properties. Springer-Verlag, Durability, pp. 225–315. https://doi.org/10.1007/978-3-642-14475-2.
Straube, J., Schumacher, C., Mensinga, P., 2010. Assessing the Freeze- Thaw Resistance of Clay Brick for Interior Insulation Retrofit Projects, in: Buildings XI International Conference. Clearwater, Florida.
Strunden, J., Ehlers, T.A., Brehm, D., Nettesheim, M., 2015. Spatial and temporal variations in rockfall determined from TLS measurements in a deglaciated valley, Switzerland. J. Geophys. Res. Earth Surf. 120, 1251–1273. https://doi.org/10.1002/2014JF003274.
Style, R.W., Peppin, S.S.L., 2012. The kinetics of ice-lens growth in porous media. J. Fluid Mech. 692, 482–498. https://doi.org/10.1017/jfm.2011.545.
Style, R.W., Peppin, S.S.L., Cocks, A.C.F., Wettlaufer, J.S., 2011. Ice-lens formation and geometrical supercooling in soils and other colloidal materials. Phys. Rev. E - Stat. Nonlinear, Soft Matter Phys. https://doi.org/10.1103/PhysRevE.84.041402.
Sun, Z., Scherer, G.W., 2008. Kinetics of ice growth in cement and concrete. In: International RILEM Symposium on Concrete Modelling, pp. 183–190.
Sun, Z., Scherer, G.W., 2010a. Effect of air voids on salt scaling and internal freezing. Cem. Concr. Res. 40, 260–270. https://doi.org/10.1016/j.cemconres.2009.09.027.
Sun, Z., Scherer, G.W., 2010b. Pore size and shape in mortar by thermoporometry. Cem. Concr. Res. 40, 740–751. https://doi.org/10.1016/J.CEMCONRES.2009.11.011.
Sun, W., Zhang, Y.M., Yan, H.D., Mu, R., 1999. Damage and damage resistance of high strength concrete under the action of load and freeze-thaw cycles. Cem. Concr. Res. 29, 1519–1523. https://doi.org/10.1016/S0008-8846(99)00097-6.
Suzuki, T., Ogata, H., Takada, R., Aoki, M., 2010. Use of acoustic emission and X-ray computed tomography for damage evaluation of freeze-thawed concrete. Constr. Build. Mater. 24, 2347–2352. https://doi.org/10.1016/J.CONBUILDMAT.2010.05.005.
Swainson, I.P., Schulson, E.M., 2001. A neutron diffraction study of ice and water within a hardened cement paste during freeze–thaw. Cem. Concr. Res. 31, 1821–1830.
Taber, S., 1916. The growth of crystals under external pressure. Am. J. Sci. 246, 532–556.
Taber, S., 1929. Frost Heaving. J. Geol. 37, 428–461. https://doi.org/10.1086/623637.
Taber, S., 1930. The Mechanics of Frost Heaving. J. Geol. 38, 303–317. https://doi.org/10.1086/623720.
Thomachot, C., Jeannette, D., 2002. Evolution of the petrophysical properties of two types of Alsatian sandstone subjected to simulated freeze-thaw conditions. Geol. Soc. London. Spec. Publ. 205, 19–32. https://doi.org/10.1144/GSL.SP.2002.205.01.03.
Thomachot, C., Matsuoka, N., 2007. Dilation of building materials submitted to frost action. Geol. Soc. Lond. Spec. Publ. 271, 167–177. https://doi.org/10.1144/GSL.SP.2007.271.01.17.
Thomachot, C., Matsuoka, N., Kuchitsu, N., Morii, M., 2005. Frost damage of bricks composing a railway tunnel monument in Central Japan: field monitoring and laboratory simulation. Nat. Hazards Earth Syst. Sci. 5, 465–476.
Thomachot-Schneider, C., Huby, E., Chalons, K., Drothière, X., Vazquez, P., 2018. Role of the capillary fringe on the dilatation of a low porosity limestone submitted to unidirectional freezing. Prog. Earth Planet. Sci. 5, 1–9. https://doi.org/10.1186/s40645-018-0213-6.
Todak, H.N., Tsui, M., Ley, M.T., Weiss, W.J., 2017. Evaluating freeze-thaw damage in concrete with acoustic emissions and ultrasonics. In: Springer Proceedings in Physics. Springer, pp. 175–189. https://doi.org/10.1007/978-3-319-29052-2_16.
Uygunoglu, T., Topcu, I.B., 2009. Thermal expansion of self-consolidating normal and lightweight aggregate concrete at elevated temperature. Constr. Build. Mater. 23, 3063–3069. https://doi.org/10.1016/j.conbuildmat.2009.04.004.
Vandemeulebroucke, I., Calle, K., Caluwaerts, S., De Kock, T., Van Den Bossche, N., 2019. Does historic construction suffer or benefit from the urban heat island effect in Ghent and global warming across Europe? Can. J. Civ. Eng. https://doi.org/10.1139/cjce-2018-0594. cjce-2018-0594.
Vehling, L., Rohn, J., Moser, M., 2016. Quantification of small magnitude rockfall processes at a proglacial high mountain site, Gepatsch glacier (Tyrol, Austria). Z. Geomorphol. 60, 93–108. https://doi.org/10.1127/zfg_suppl/2015/S-00184.
Vehling, L., Rohn, J., Moser, M., 2019. Rockfall at Proglacial Rockwalls—A Case Study from the Kaunertal, Austria. Springer, Cham, pp. 143–156. https://doi.org/10.1007/978-3-319-94184-4_9.
Vereecken, E., Van Gelder, L., Janssen, H., Roels, S., 2015. Interior insulation for wall retrofitting – a probabilistic analysis of energy savings and hygrothermal risks. Energy Build. 89, 231–244. https://doi.org/10.1016/j.enbuild.2014.12.031.
Verstrynge, E., De Wilder, K., Drougkas, A., Voet, E., Van Balen, K., Wevers, M., 2018. Crack monitoring in historical masonry with distributed strain and acoustic emission sensing techniques. Constr. Build. Mater. 162, 898–907. https://doi.org/10.1016/J.CONBUILDMAT.2018.01.103.
Vosteen, H.-D., Schellschmidt, R., 2003. Influence of temperature on thermal conductivity, thermal capacity and thermal diffusivity for different types of rock. Phys. Chem. Earth, Parts A/B/C 28, 499–509. https://doi.org/10.1016/S1474-7065(03)00069-X.
Walder, J., Hallet, B., 1985. A theoretical model of the fracture of rock during freezing. Geol. Soc. Am. Bull. 96, 336–346.
Wardeh, G., Perrin, B., 2008. Numerical modelling of the behaviour of consolidated porous media exposed to frost action. Constr. Build. Mater. 22, 600–608. https://doi.org/10.1016/J.CONBUILDMAT.2006.11.001.
Watanabe, T., Matsuoka, N., Christiansen, H.H., 2012. Mudboil and ice-wedge dynamics investigated by electrical resistivity tomography, ground temperatures and surface movements in Svalbard. Geogr. Ann. Ser. A Phys. Geogr. 94, 445–457. https://doi.org/10.1111/j.1468-0459.2012.00470.x.
Webber, J.B.W., Dore, J.C., Strange, J.H., Anderson, R., Tohidi, B., 2007. Plastic ice in confined geometry: the evidence from neutron diffraction and NMR relaxation. J. Phys. Condens. Matter 19, 12. https://doi.org/10.1088/0953-8984/19/41/415117.
Weber, S., Faillettaz, J., Meyer, M., Beutel, J., Vieli, A., 2018. Acoustic and microseismic characterization in steep bedrock permafrost on matterhorn (CH). J. Geophys. Res. Earth Surf. 123, 1363–1385. https://doi.org/10.1029/2018JF004615.
Winkler, E.M., 1968. Frost damage to stone and concrete: geological considerations. Eng. Geol. 2, 315–323.
Yavuz, H., 2011. Effect of freeze–thaw and thermal shock weathering on the physical and mechanical properties of an andesite stone. Bull. Eng. Geol. Environ. 70, 187–192. https://doi.org/10.1007/s10064-010-0302-2.
Yavuz, H., Altindag, R., Sarac, S., Ugur, I., Sengun, N., 2006. Estimating the index properties of deteriorated carbonate rocks due to freeze–thaw and thermal shock weathering. Int. J. Rock Mech. Min. Sci. 43, 767–775. https://doi.org/10.1016/J.IJRMMS.2005.12.004.
Zhou, X., Derome, D., Carmeliet, J., 2017. Hygrothermal modeling and evaluation of freeze-thaw damage risk of masonry walls retrofitted with internal insulation. Build. Environ. 125, 285–298. https://doi.org/10.1016/J.BUILDENV.2017.08.001.
Zuber, B., Marchand, J., 2000. Modeling the deterioration of hydrated cement systems exposed to frost action: part 1: Description of the mathematical model. Cem. Concr. Res. 30, 1929–1939. https://doi.org/10.1016/S0008-8846(00)00405-1.